



Everything Is Everywhere: Physiological Responses of the Mediterranean Sea and Eastern Pacific Ocean Epiphyte *Cobetia* Sp. to Varying Nutrient Concentration

Víctor Fernández-Juárez¹ · Daniel Jaén-Luchoro^{2,3} · Jocelyn Brito-Echeverría⁴ · Nona S. R. Agawin¹ · Antoni Bennasar-Figueras⁵ · Pedro Echeveste^{4,6}

Received: 24 October 2020 / Accepted: 22 April 2021

© The Author(s), under exclusive licence to Springer Science+Business Media, LLC, part of Springer Nature 2021

Abstract

Bacteria are essential in the maintenance and sustainment of marine environments (e.g., benthic systems), playing a key role in marine food webs and nutrient cycling. These microorganisms can live associated as epiphytic or endophytic populations with superior organisms with valuable ecological functions, e.g., seagrasses. Here, we isolated, identified, sequenced, and exposed two strains of the same species (i.e., identified as *Cobetia* sp.) from two different marine environments to different nutrient regimes using batch cultures: (1) *Cobetia* sp. UIB 001 from the endemic Mediterranean seagrass *Posidonia oceanica* and (2) *Cobetia* sp. 4B UA from the endemic Humboldt Current System (HCS) seagrass *Heterozostera chilensis*. From our physiological studies, both strains behaved as bacteria capable to cope with different nutrient and pH regimes, i.e., N, P, and Fe combined with different pH levels, both in long-term (12 days (d)) and short-term studies (4 d/96 h (h)). We showed that the isolated strains were sensitive to the N source (inorganic and organic) at low and high concentrations and low pH levels. Low availability of phosphorus (P) and Fe had a negative independent effect on growth, especially in the long-term studies. The strain UIB 001 showed a better adaptation to low nutrient concentrations, being a potential N₂-fixer, reaching higher growth rates (μ) than the HCS strain. P-acquisition mechanisms were deeply investigated at the enzymatic (i.e., alkaline phosphatase activity, APA) and structural level (e.g., alkaline phosphatase D, PhoD). Finally, these results were complemented with the study of biochemical markers, i.e., reactive oxygen species (ROS). In short, we present how ecological niches (i.e., MS and HCS) might determine, select, and modify the genomic and phenotypic features of the same bacterial species (i.e., *Cobetia* spp.) found in different marine environments, pointing to a direct correlation between adaptability and oligotrophy of seawater.

Keywords *Posidonia oceanica* · *Heterozostera chilensis* · Mediterranean Sea · Humboldt Current System · *Cobetia* sp. (UIB 001 and 4B UA) and nitrogen (N)-phosphorus (P)-iron (Fe) regimes

✉ Víctor Fernández-Juárez
victorfj@hotmail.es

¹ Marine Ecology and Systematics (MarES), Department of Biology, University of the Balearic Islands, Palma, Spain

² Department of Infectious Diseases, Sahlgrenska Academy, University of Gothenburg, Gothenburg, Sweden

³ Culture Collection University of Gothenburg (CCUG), Sahlgrenska Academy of the University of Gothenburg, Gothenburg, Sweden

⁴ Instituto de Ciencias Naturales Alexander von Humboldt, Universidad de Antofagasta, Antofagasta, Chile

⁵ Grup de Microbiologia, Department of Biology, University of the Balearic Islands, Palma, Spain

⁶ Instituto Milenio de Oceanografía, Concepción, Chile

Introduction

Seagrasses are one of the most productive ecosystems, placed in continental seashores of all continents but Antarctica [1], providing key ecological services. As relevant coastal primary producers, seagrasses fix atmospheric CO₂, acting as carbon sinks and O₂ releasers. They also sustain secondary production, trap particles, stabilize sediments, are key actors of biogeochemical processes (e.g., nitrogen cycles), and form the habitat and nursery for several micro- and macro-organisms [2]. Their associated microbiome takes part in the major ocean's biogeochemical cycles (e.g., nutrient cycling of nitrogen (N), phosphorus (P), and/or iron (Fe)) and microbial food webs [3–5], essential for the livelihood of seagrasses. Within the bacterial consortia, primary producers (e.g.,

Prochlorococcus and *Synechococcus*) play a critical role through their CO₂-fixing capacity [6], together with other bacteria in sulfide detoxification (which is highly toxic for plant growth [7]), and biological N₂-fixation (BNF) which compensates denitrification, converting dinitrogen gas (N₂) to inorganic N (i.e., ammonia, NH₃) [8]. The role of environmental factors (e.g., nutrient availability) modulating bacterial community composition, diversity, functioning, and, thus, the health and productivity of the seagrasses, remains to be investigated.

The implication of the microbial communities associated with seagrasses, which can be found as epiphytic or endophytic, has been profusely illustrated on the Mediterranean endemic seagrass *Posidonia oceanica* (L.) Delile [9–11]. N₂-fixers or diazotrophs can supply the entire N-demand of the plant, having a key role in nutrient cycling [12], considering the Mediterranean Sea (MS) oligotrophy. The MS is a semi-enclosed sea chronically limited by P [13], where P and N concentrations do not obey the Redfield ratio (i.e., 23–28:1) [14, 15]. Besides, Mediterranean waters are subjected to Saharan atmospheric dust deposition, which controls Fe concentrations in the water column [16]. On the other hand, the Humboldt Current System (HCS), which extends from the west coast of South America (Southern Chile) up to Ecuador and the Galapagos Islands, is one of the most productive marine ecosystems as a result of the transport of sub-Antarctic-enriched nutrient waters and often poor in Fe [17–19]. There, the endemic *Heterozostera chilensis* J. Kou seagrass thrives settled after long-distance dispersion of its ancestor, i.e., *Heterozostera nigricaulis*, from temperate waters of Australia across the Pacific Ocean [20, 21]. Noteworthy, it is intriguing how *H. chilensis* (former *H. nigricaulis*) was capable to settle in the cold waters of the HCS, concretely in Puerto Aldea, Bahia Chascos, and Isla Damas [21], where historically seaweeds have proliferated, but no seagrasses [22]. Among the many intrinsic characteristics that may have allowed *H. chilensis* to survive, the role of its associated microbiota in its maintenance and sustenance remains unclear.

Elucidating the nutrient regimes of N, P, and Fe of these microbial communities is of especial relevance as they limit microbial growth and activity [17], usually controlled by upwelling/downwelling processes or by atmospheric dust deposition [23]. The average ratio of N/P/Fe in microbial communities obeys to Redfield ratio, 16 (N):1 (P):0.0075 (Fe), and hence N and P are the major elements needed for microbial biomass, constituting around 7% and 1% of cell biomass, respectively [24, 25]. In P-limited waters, bacteria are capable of hydrolyzing P-esters contained in dissolved organic phosphorus (DOP) releasing dissolved inorganic phosphorus (DIP), through the so-called alkaline phosphatases (APases). Bacterial APases can be classified into three main families depending on the associated co-factor (i.e., Mg²⁺, Zn²⁺, Fe³⁺, and/or Ca²⁺): PhoA, PhoX, and PhoD [26]. Thus,

metals, as Fe, are essential for enzyme activity as structural components. Nonetheless, Fe homeostasis has to be tightly regulated since it can promote oxidative stress by the generation of reactive oxygen species (ROS) through Fenton and Haber-Weiss reactions [27].

Multifactorial studies investigating the interactive effects of N, P, and Fe in marine microorganisms are very scarce [28–31]. Low dissolved inorganic N (DIN, e.g., NO₃⁻), inorganic P (PO₄³⁻), and Fe concentrations can impair growth, enhancing oxidative stress, morphological changes, and apoptosis processes, as well as limiting N₂-fixation rates [31]. In oligotrophic waters (e.g., North Atlantic Ocean or the MS), Fe can limit P-mechanisms as the alkaline phosphatase activity (APA) [32], and APA can be subjected to DIN concentration [30]. In the global ocean, microbial communities are faced with a wide range of nutrient regimes (e.g., from oligotrophy to eutrophic) and abiotic scenarios, selecting the best-adapted species worldwide [33]. Analyzing the biogeographic patterns of cosmopolitan species is of special relevance to better address the success of these species in adapting and surviving to a wide range of scenarios, an issue poorly studied with bacteria associated with seagrasses.

Gammaproteobacteria is one of the most distributed marine heterotrophic bacteria in the oceans [34]. Among them, the *Halomonadaceae* family (which include *Modicisalibacter*, *Halotalea*, *Zymobacter*, *Carnimonas*, *Cobetia*, *Kushneria*, and *Salinicola*) is found in almost any saline environment, being moderate halophilic bacteria and exopolysaccharides producers [35, 36]. As a result of the re-classification of the *Halomonas marina*, Arahal et al. (2002) described the genus *Cobetia* as a member of the *Halomonadaceae* [20], which comprises five species (i.e., *C. amphilecti*, *C. crustatorum*, *C. lioralis*, *C. marina*, and *C. pacifica*) [37–39]. *Cobetia* spp. are isolated as hydrocarbon-degrading, biosurfactants-producing, which display a nutritional versatility and different metabolic profiles (e.g., sugar utilization and assimilation), being sources of psychrophile enzymes. Besides, some strains have a key role in improving the water quality [40–43]. Although the ecophysiology and adaptation responses of *Cobetia* spp. remains poorly explored, the genus *Cobetia* is well distributed throughout the world oceans having been isolated from different marine ecological niches, pointing to their high adaptability.

Our genomic analysis proved that we isolated two strains that belong to the same species, inside the genus *Cobetia*, placed in geographically unrelated endemic seagrasses: *P. oceanica* from the MS and *H. chilensis* from the HCS. Based on our previous studies in which we described the sensitivity of the diazotrophic bacteria to different nutrient regimes and emerging pollutants [30, 31, 44], the aim of this study, considering the contrasting features of the MS and HCS at nutrient level, was to evaluate the physiological responses of the *Cobetia* spp. isolated, using batch cultures. For this

purpose, we conducted long-term (i.e., 12 days (d)) and short-term experiments (i.e., 4 d/96 h) towards different nutrient regimes (i.e., N, P, and Fe) and pH levels, measuring their physiological and biochemical responses.

Materials and Methods

Isolation, Sequencing, Identification, and Genomic Features of UIB 001 and 4B UA Strains

Isolation of the Strains

The strains UIB 001 and 4B UA were isolated from the roots of *P. oceanica* and leaves of *H. chilensis*, respectively. *Posidonia oceanica* roots were collected from Cala Nova (Mallorca) in Balearic Islands, Spain (39° 33' 02.3" N 2° 36' 02.1" E), while *H. chilensis* leaves were collected from the seashore of Puerto Aldea (Coquimbo), Chile (30° 17' 37.83" S–71° 36' 24.55" O). *Posidonia oceanica* roots were triturated in Tris-EDTA 1 mM pH 7.5, whereas *H. chilensis* leaves were rasped to gather the epiphytic community, which was maintained in sterile seawater. In both cases, the microbial consortia were cultured in modified artificial seawater (ASW) medium (L⁻¹: 25.0 g NaCl, 1.0 g MgCl₂·6H₂O, 5.0 g MgSO₄·7H₂O, 0.7 g KCl, 0.15 g CaCl₂·2H₂O, 0.1 g KBr, 0.04 g SrCl₂·6H₂O, and 0.025 g H₃BO₃), with 1 ml L⁻¹ trace metal [L⁻¹: 2.86 g H₃BO₃, 1.81 g MnCl₂·4 H₂O, 0.22 g ZnSO₄·7H₂O, 0.39 g NaMoO₄·2H₂O, 0.079 g CuSO₄·5H₂O, and 0.049 g Co(NO₃)₂·6H₂O], glucose/citrate (final concentration 0.1% (v/v)), and with agarose (1.5% (p/v)). Cultures had N₂ as sole N source (with low P and Fe concentrations) and were incubated at 20 °C. The resulting colonies were subcultured in marine agar (MA) to obtain pure cultures.

Genome Sequencing

Total genomic DNA of the strains UIB 001 and 4B UA were extracted using the optimized version of Salvà Serra et al. (2018) [45]. Illumina whole-genome sequencing was performed (Eurofins Scientific, Luxemburg). Briefly, the DNA libraries were prepared following an optimized protocol and standard Illumina adapter sequences. Paired-end sequences were determined using the Illumina HiSeq platform (read mode, 2 × 150 bp). Additionally, DNAs were sequenced with a MinION Mk101B sequencer (Oxford Nanopore Technologies, Oxford, UK) for the generation of long-read sequences. The DNA library was prepared, using the rapid barcoding sequencing kit vR9 (SKQ-RBK004) and loaded into a FLO-MIN106 vR9.4 flow cell. The sequencing process was performed for 48 h (h) on MinKNOW software v1.4.2 (Oxford Nanopore Technologies). The raw reads obtained were base called using Guppy software v3.5.1 (Oxford

Nanopore Technologies). Quality of Illumina and nanopore reads were determined using fastQC (<https://www.bioinformatics.babraham.ac.uk/projects/fastqc/>) and NanoPlot software (<https://github.com/wdecoster/NanoPlot>), respectively. A hybrid assembly was done using Unicycler v0.4.7 [46] combining the Illumina and nanopore reads. The qualities of the genome sequences obtained were assessed using the Quality Assessment Tool for Genome Assemblies (QUAST) v4.5 [47]. For submission to GenBank, the whole-genome sequences were annotated with the Prokaryotic Genome Annotation Pipeline (PGAP) [48, 49].

Strain Identification

Complete 16S rRNA gene sequences were extracted from the obtained genomes and analyzed using EzBioCloud to determine the closely related species [50]. Afterward, the genome sequences of the strains UIB 001 and 4B UA were compared with the genomes of the closely related species, which were obtained from NCBI. Comparative 16S rRNA gene sequence analyses were done using the Kimura two-parameter model to calculate evolutionary distances. Cluster analyses and phylogenetic trees were built by Neighbor-Joining, using the MEGA7 software [51]. Bootstrap values were determined for 1000 replications. Average nucleotide identities by BLAST (ANIb) were determined using the JSpeciesWS tool [52]. The digital DNA–DNA hybridization (dDDH) similarity values were determined with the Genome-to-Genome Distance Calculator (GGDC) [53]. Only results of the recommended formula 2 (sum of all identities found in high-scoring segment pairs (HSPs) divided by the overall HSP length) in the GGDC analyses were considered.

Genomic Difference Detection Through Pan-Genome Analysis and Single Nucleotide Polymorphisms (SNPs)

Pan-genome analysis was performed following an already described procedure [54]. Briefly, homologous determinations were performed using the software Get_Homologues [55], based on two different algorithms: Cluster of Orthologous Genes Triangle (COGT) and Orthologous Markov Cluster (OMCL). The total number of clusters conforming the pan-genome was determined with the consensus of COGT and OMCL. Exclusive proteins of each strain, extracted from the pan-genome determination, were assigned to a functional category using the eggNOG-mapper v2 online tool [56]. Single nucleotide polymorphism (SNPs) analyses were done using Snippy (<https://github.com/tseemann/snippy>), using the default parameters and the genome of strain UIB 001 as a reference.

Experimental Design

Prior to the experiments, temperature (4–42 °C) and NaCl tolerance (0–20% (p/v)) were tested. Besides, biochemical tests were carried out in the Spanish Type Culture Collection (CECT) using API 20NE and API ZYM test kits (Biomérieux), following the manufacturer's instructions and adding Marine Cations Supplement in a 1/10 ratio, and incubated at 30 °C. To evaluate their ability to cope with different nutrient regimes and changes in cell morphology, bacterial cells were grown in ASW with agarose (1.5% (p/v)), containing optimal nutrients (+N, +P, +Fe, and +carbon source (C)), N₂ as sole N source (–N, +P, +Fe, and +C), without P and Fe (+N, –P, –Fe, and +C), without N, P, and Fe (–N, –P, –Fe, and +C), with N, P, Fe, and not C (+N, +P, +Fe, and –C), and without N, P, Fe, and C (–N, –P, –Fe, and –C).

Cobetia sp. isolates were cultured and acclimatized in marine broth (MB) at 20 °C and 150 r.p.m. The subcultures for seeding were centrifuged and washed with their corresponding medium without N, P, and Fe. All the experiments were performed in triplicate in sterile 50 mL Falcon tubes and/or 2 mL microplates in modified ASW culture media (without agarose), in batch cultures. We inoculated 7×10^5 cell mL⁻¹ in each treatment. Samples were manipulated in a glass-clean hood to avoid Fe contamination, and cultures were maintained over 4–12 d, at 20 °C and 120 r.p.m.

Different inorganic/organic N (i.e., NH₃ from NH₄Cl and/or C₄H₁₁NO₃ [Tris]), inorganic P (i.e., PO₄³⁻ from K₂HPO₄), and Fe (from ferric citrate [C₆H₅FeO₇]) concentrations were tested at different pH (6–8), as shown in the Supplementary Table S1, based in previous works [30, 31]. Briefly, for N, four levels of inorganic (NH₃) and/or organic N (Tris) were tested: Non-N [0 mM], 0.8 mM NH₃, 1 mM Tris, and 1 mM Tris +0.8 mM NH₃; for PO₄³⁻, two levels were tested: [Low PO₄³⁻, 0.005 μM] and [High PO₄³⁻, 50 μM], as well as for Fe, [Low Fe, 1 nM] and [High Fe, 1 μM]. All these concentrations were combined in three different experimental designs: (I) long-term studies (12 days) performing growth curves (where growth rates (μ) and duplication times (T_g) were measured) at pH 8 and (II) and (III) short-term studies (96 h), testing N, and PO₄³⁻ concentration effects at different pH levels, respectively. During the experiment, subsamples were taken to measure growth, alkaline phosphatase activity (APA), and reactive oxygen species (ROS). Besides, (IV) we measured APA under different levels of PO₄³⁻ (0.005–100 μM) and Fe (1 nM and 1 μM) at pH 8 after 96 h (Supplementary Table S1).

Flow Cytometry and Growth Responses

Flow cytometry was used to assess changes in cell abundances. For long-term studies, subsamples of the culture (1.5 mL) were daily sampled, fixed with 36% (p/v) of formalin and froze at –20 °C until reading at the end of the

experiments. For the rest of the experiments, measurements were performed without freezing nor fixing. The cytometer used was the BD FACSJazz™, previously calibrated with the SPHEROTM Ultra Rainbow Fluorescent Particles, 3.08 μm. The cells were separated by adjusting the voltages, according to size and complexity: forward scatter (FCS) versus side scatter (SSC), respectively. Cell counts were adjusted to count for 10 s or 1000,000 events. To measure the growth rates (μ) and duplication times (T_g), we followed the equations used in Fernández-Juárez et al. (2020) [31]. To evaluate the effect of the low nutrient concentration (i.e., serial, simultaneous, or independent) of the growth response to P and Fe (with N replete), the log ratio effect-size criteria based on the mean treatment and control response was assessed as in Fernández-Juárez et al. (2020) [31].

Microscopical Analysis

Microscopical images were taken with the Leica TCS SPE confocal microscope, Leica Microsystems. The samples were placed on a clean slide with DAPI at a final concentration of 0.1 mg mL⁻¹. The samples were kept in the dark until reading, taking the images with the ×100 objective combining the brief-field I (BF) channel. Images were processed with ImageJ software, and cell volume was calculated following Hillebrand et al. (1999) [57].

Alkaline Phosphatase Activity

Alkaline phosphatase activity (APA) was evaluated using a fluorometric assay and following the MUF-P hydrolysis [30]. At the end of the experiment, APA was tested at low levels of PO₄³⁻ (i.e., 0.005 μM) with low or high levels of Fe (1 nM or 1 μM) combined with different pH levels (pH 6–8). Moreover, a battery of concentrations of PO₄³⁻ (0.005, 0.05, 0.5, 5, 50, and 100 μM) combined with different levels of Fe (1 nM and 1 μM) at pH 8 was performed (Supplementary Table S1). An endpoint assay was conducted, using 5 μM MUF-P. After 1 h of incubation in darkness at room temperature, APA was measured in a microtiter plate that contained buffer borate pH 10 (3:1 of sample: buffer). With a Cary Eclipse spectrofluorometer (FL0902M009, Agilent Technologies), MUF production (fmol MUF cell⁻¹ h⁻¹) was measured at 359 nm (excitation) and 449 nm (emission), using a calibration standard curve with commercial MUF (Sigma-Aldrich). Results were normalized by cell number.

Structural Analysis of the Alkaline Phosphatase

Sequences of PhoD of the UIB 001 and 4B UA (locus_tag: HA399_02660 and H2O77_02640) in FASTA format were sent to the I-Tasser server for protein 3D-structure prediction [58], with their domains previously checked in Pfam 32.0

[59]. The predicted structures were sent to POSA for a structural alignment between them [60]. The description of the Ca²⁺ and Fe³⁺ coordination positions of these proteins was based on the descriptions of the catalytic center of the PhoD from *C. amphilecti* KMM 296 (WP_043333989) [61] and the PhoD crystal structure of *Bacillus subtilis* (PDB: 2YEQ). Residues from PhoD from UIB 001 and 4B UA strains against the PhoD of *C. amphilecti* KMM 296 were mapped through alignments with Uniprot Clustal Omega [62]. The predicted structures and the corresponding structural alignments were visualized with Pymol [63].

Reactive Oxygen Species Production

ROS detection was measured with the molecular probe 2',7'-dichlorofluorescein diacetate (DCFH-DA, Sigma) [31]. Briefly, bacterial samples were placed in a 96-well microplate (Thermo Scientific) spiked with DCFH-DA at a final concentration of 15 µg mL⁻¹. The green fluorescence product, 2',7'-dichlorofluorescein (DCF), generated after its oxidation by ROS was measured at 25 °C in the Eclipse spectrofluorometer (FL0902M009, Agilent Technologies) for 1 h with an excitation of 480 nm and emission of 530 nm. The results were expressed as the slope of the linear regression obtained and normalized by cell (arbitrary units [AU] cell⁻¹). DCFH-DA was added in ASW without cells as blanks under the same conditions.

Statistical Analysis

A parametric univariate analysis of variance (ANOVA) factor and post hoc (Bonferroni) was used to study the effect of N, P, and Fe concentrations in the UIB 001 and 4B UA strains. The statistical analyses were performed using the SPSS software v21 (IBM Corp year 2012).

Results

Characterizing *Cobetia* Sp. UIB 001 and 4B UA

Genomic Analyses

Based on 16S rRNA, ANIb, and GGDC analyses, we revealed that both strains from the endemic Mediterranean seagrass *P. oceanica* and the endemic HCS seagrass *H. chilensis*, respectively, corresponded to the same species and belonging to the *Cobetia* genus (Table 1, Fig. 1, Supplementary Tables S2, S3 and S4). The 16s rRNA analysis of the UIB 001 and 4B UA strains showed a similarity between 99.5 and 99.9% with the type strains *C. amphilecti* KMM 1516^T, *C. litoralis* KMM 3880^T, *Cobetia marina* JCM 21022^T, and *C. pacifica* KMM 3879^T (Supplementary Table S2). Besides, the 16S rRNA

phylogenetic tree showed a clade formed by these species, supported with high bootstrap values (Fig. 1). Based on these results, the UIB 001 and 4B UA strains seem to be more closely related to *C. amphilecti* and *C. litoralis* (Supplementary Table S2). In agreement with the 16s rRNA analysis, ANIb and DDH analyses also confirmed that strains UIB 001 and 4B UA belong to the same species, showing a similarity over 96% (ANIb) and 70% (dDDH) between them (Table 1 and Supplementary Tables S3 and S4). Comparisons with genomes of the *Cobetia* genus present in GenBank were carried out to provide deeper insights into their taxonomic affiliation (Supplementary Table S3 and S4). There is an important lack of genome sequences of type strains inside the *Cobetia* genus, being *C. marina* the unique species for which the type strain has been genome sequenced (JCM 21022^T, accession number CP017114). The genome of *C. amphilecti* KMM 296, which is not the type strain, showed the highest score by ANIb and dDDH (over 96 and 70%, respectively), indicating that, presumably, our strains might be representatives of *C. amphilecti* (Supplementary Tables S3 and S4). However, due to the lack of type strain genomic information, it was not possible to perform an accurate final taxonomic classification at the species level. Overall, with our results, we can affirm that the strains isolated belong to the *Cobetia* genus, and they are not *C. marina*. Thus, the strains were named *Cobetia* sp. UIB 001 and 4B UA.

Genomic Features

Sequencing and assembly procedures generated two complete and closed genomes. The genome sequence of the strain UIB 001 was composed of one chromosome (4,177,647 bp) and one putative plasmid (10,679 bp), while the genome of strain 4B UA was composed of one chromosome (4,319,205 bp) and two putative plasmids (4702 and 2015 bp). The main genomic features of each genome are included in Table 1 and Fig. 2A and B. The complete genome sequences were deposited at DDBJ/EMBL/GenBank under the accession numbers CP058244 to CP058245 (*Cobetia* sp. UIB 001) and CP059843 to CP059845 (*Cobetia* sp. 4B UA).

Genomic Differences

The pan-genome analysis determined that both strains shared 3087 homologous proteins (Fig. 3A). Functional analysis of the entire set of proteins of each strain displayed that both strains shared almost the same distribution of gene functions (Supplementary Fig. S1). Additionally, 197 proteins were exclusively present in the strain UIB 001, whereas the strain 4B UA had 278 specific proteins (Fig. 3A). It is worth mentioning that the functional category with the most representatives was "Function unknown" (Fig. 3B). Results from the SNPs

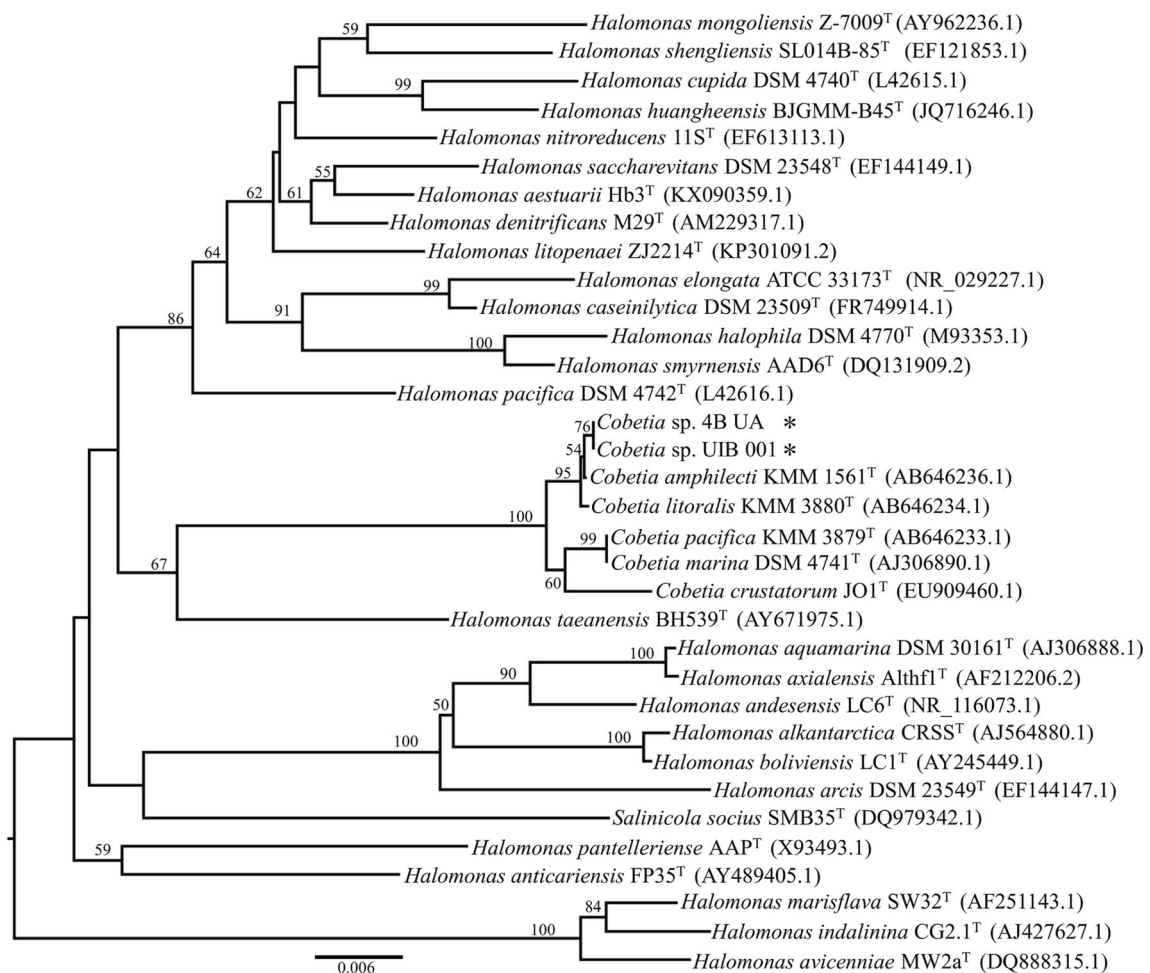
Table 1 Genomic features of *Cobetia* sp. UIB 001 and 4B UA

	UIB 001	4B UA
Genome length (bp)	4,177,647	4,319,205
G+C (%)	62.78%	62.56%
Genes	3488	3562
Protein-coding genes	3391	3474
rRNA operons	7	7
tRNA genes	74	72
Putative plasmids	1 (10,679 bp)	2 (4702 and 2015 bp)
16s rRNA identity (% between each other)	100%	100%
ANib (% between each other)	96.99%	96.93%
dDDH (% between each other)	75.80	75.80%

analysis showed up to 66,929 SNPs between both strains. Among the “classical” proteins implicated in the adaptation and survival to low N, P, and Fe availability, we detected up to 1045 SNPs, 470 SNPs for proteins related to N-metabolism, 277 SNPs for proteins related to P-metabolism, and 298 SNPs for proteins related to Fe-metabolism (Fig. 3C).

Phenotypic Features

From the phenotypic point of view, these rod-shaped bacteria (1–1.5 μm length and 0.7–0.8 μm width) were able to grow in nutrient-depleted media, i.e., in N-, P-, and Fe-depleted solid media (with 1.5% (p/v) agarose), as long as carbon (C)

**Fig. 1** Complete 16S rDNA phylogenetic tree of *Cobetia* spp. and other closely related groups, including the strains *Cobetia* sp. UIB 001 and 4B UA (*)

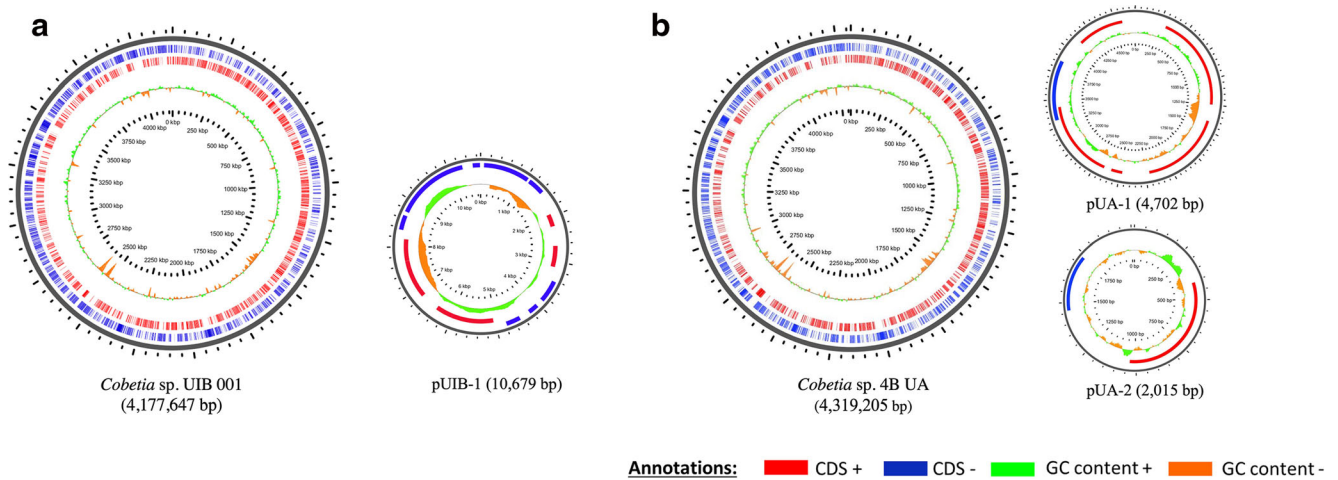


Fig. 2 Genome BLAST atlas of the chromosomes for the strains **A** UIB 001 and **B** 4B UA, showing the overall similarity of the chromosome organization between them. Position of CDS+ and CDS-, as well as GC content, is indicated

source was present (Table 2). In agreement with the species more related to them (*C. amphilecti* KMM 1516^T and *C. litoralis* KMM 3880^T), both isolated had a tolerance over 15% NaCl (yet growth was not detected at 20%

NaCl) and up to 42 °C (Table 2). Overall, biochemical tests showed that both *Cobetia* sp., UIB 001 and 4B UA, had the same metabolic profiles and similar to the most related type strains (Table 2).

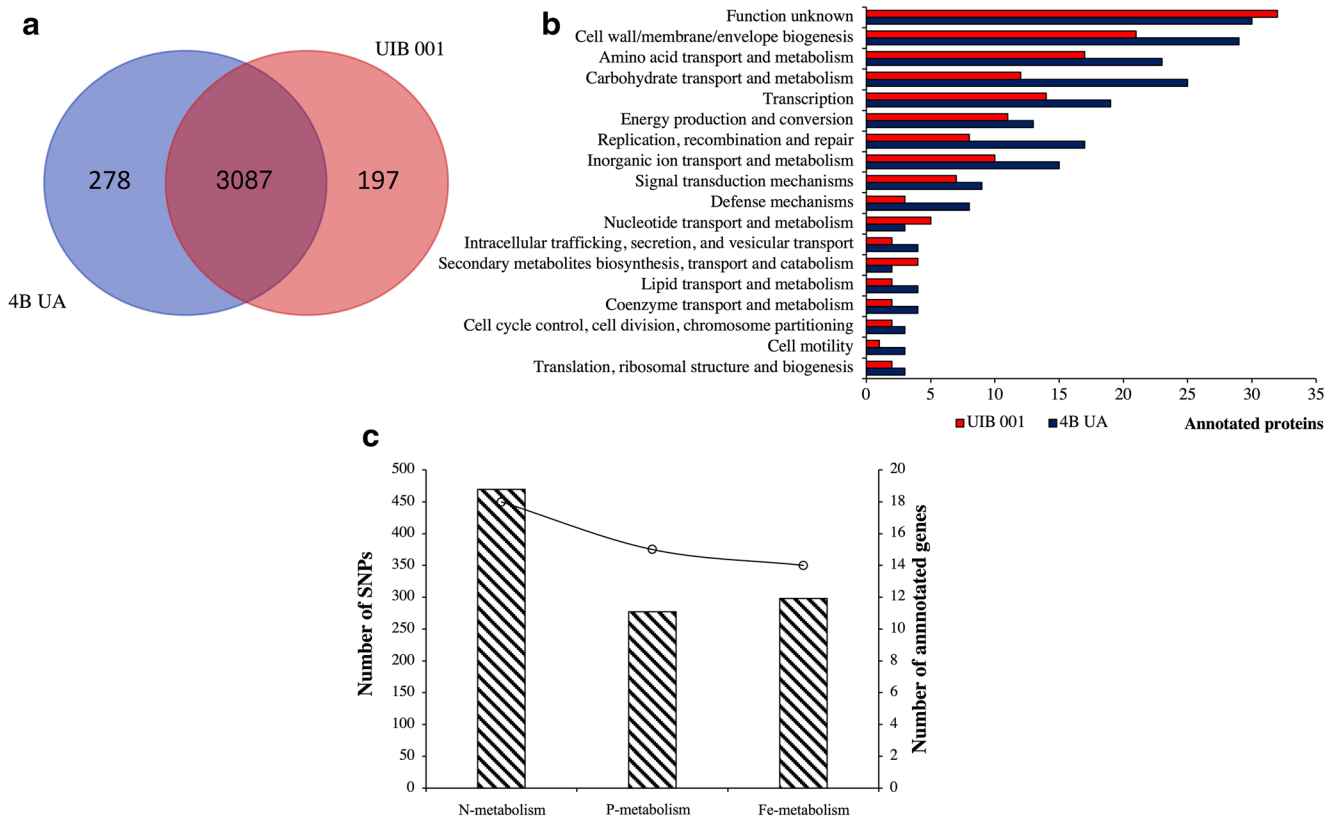


Fig. 3 Genomic differences between *Cobetia* sp. UIB 001 and 4B UA. **A** Pan-genomic analysis between *Cobetia* sp. UIB 001 and 4B UA, showing the number of shared proteins between the strains, as well as the number of exclusive proteins of each strain. **B** Functional categorization by COG

analyses of the exclusive proteins of UIB 001 and 4B UA strains. **C** Number of SNPs detected in genes implicated in N, P, and Fe metabolism. The bar chart represents the number of SNPs, whereas, lines represent the number of annotated genes implicated in N, P, and Fe metabolism

Table 2 Differential phenotypic characteristics of the *Cobetia* sp. UIB 001 and 4B UA and the most related *Cobetia* sp. species, *Cobetia amphilecti* KMM 1516^T and *Cobetia litoralis* KMM 3880^T, whose results were obtained from Romanenko et al. (2016)

		UIB 001	4B UA	KMM 1516 ^T	KMM 3880 ^T
Habitat		Mediterranean Sea (Balearic Islands, Spain)	Humboldt Current System (Puerto Aldea, Chile)	Internal tissue of the sponge <i>Amphilectus digitatus</i> (Alaska)	Sandy sediment sample collected at a depth of 1 m from the shore of the Sea of Japan, Russia
Motility		–	–	+	+
Morphology		Rod-shaped (0.76 µm width and 1.2 µm length)	Rod-shaped (0.76 µm width and 1.1 µm length)	Rod-shaped (0.8–0.9 µm width and 1.1–1.6 µm length)	Rod-shaped (0.7–0.9 µm width and 1.8–2.2 µm length)
Growth NaCl (%)	0%	–	–	s	s
	1%	+	+	+	+
	10%	+	+	+	+
	20%	–	–	+	+
Growth (°C)	4 °C	+	+	+	+
	42 °C	+	+	+	+
Optimum pH		≈ 8	≈ 8	6.5–8.5	7.5–8.5
Growth under very low nutrient concentration	(+P+Fe+N+C)	++	++	Non-tested	Non-tested
	(–P–Fe+N+C)	++	+		
	(+P+Fe–N+C)	+	+		
	(–P–Fe–N+C)	+	+		
	(+P+Fe+N–C)	–	–		
	(–P–Fe–N–C)	–	–		
API 20NE test	PNPG test; assimilation D-glucose, D-mannitol, maltose and D-gluconate	+	+	+	+
	Nitrate reduction, indole production, glucose fermentation, arginine dihydrolase and urease activity, aesculin hydrolysis, gelatinase; assimilation of L-arabinose, N-acetylglucosamine, D-mannose	–	–	–	–
	Caprate	–	w	–	+
	Adipate	–	w	–	–
	L-Malate	w	w	+	+
	Citrate and phenylacetate	w	w	–	–
Enzyme activities (API ZYM)	Alkaline phosphate, esterase (C4), esterase lipase (C8), acid phosphatase, α-glucosidase	+	+	+	+
	naphthol-AS-BI-phosphohydrolase	–	–	–	–
	Lipase (C14), cystine arylamidase, trypsin, α-chymotrypsin, α-galactosidase, β-glucuronidase, β-glucosidase, N-acetyl-β-glucosaminidase, α-mannosidase, α-fucosidase	–	–	–	–
	Valine arylamidase, β-galactosidase	–	–	w	–

Symbols +, –, w, and s, indicate positive, negative, weak, and slow reaction, respectively

Long- and Short-Term Effects of Varying Nutrient Concentration (N, P, and Fe)

Effect on Morphology

Nitrogen, P, and Fe triggered differential responses on the morphology of the UIB 001 and 4B UA strains (Fig. 4A–I).

With N₂ as the sole N source, rod-shaped cells became more circular (≈1.2 µm length and 0.97 µm width) than under optimal nutrient conditions (≈1.16 µm length and 0.76 µm width) (Fig. 4C, D, and I). Under P/Fe or total nutrient (N, P, and Fe) depletion, cells became larger and wider (≈1.68 µm length and 0.95 µm width) than under optimal concentrations (≈1.16 µm length and 0.76 µm width) (Fig. 4E–I). Overall,

under low nutrient concentrations, both strains' volume (μm^3) significantly increased (Fig. 4I).

Changes of N Concentrations

Long-Term Effect of N Long-term studies testing N_2 as the sole N source showed differential effects between UIB 001 and 4B UA (ANOVA, $p < 0.05$, Fig. 5A and B). N-depletion for UIB 001 reduced cell growth by 3-fold (μ , 0.18 d^{-1} and T_g , 3.87 d) compared to optimal nutrient conditions (μ , 0.51 d^{-1} and T_g , 1.37 d) (Bonferroni test, $p < 0.05$, Fig. 5B). Nevertheless, UIB 001 strain was capable to grow under this condition, showing its diazotrophic features. Although we did not find any annotated *nif* genes, UIB 001 possesses a *ccb3*-type cytochrome oxidase (locus_Tag: HA399_01480) found in N_2 -fixing organisms and had active N_2 -fixation rates (Supplementary Fig. S2A).

Besides, both strains were capable of growth in Burk's N-free medium, recommended for detecting N_2 -fixing organisms [64] (Supplementary Fig. S2B).

Short-Term Effects of N along with pH Different N sources (i.e., inorganic, NH_3 , and/or organic, Tris) triggered different effects on UIB 001 and 4B UA at pH 8 after 96 h (ANOVA, $p < 0.05$, Fig. 5C). For both, increasing N sources had a positive impact, reaching the highest growths at 0.8 mM of NH_3 and 1 mM of Tris for UIB 001 and 4B UA, respectively (Fig. 5C). However, combining inorganic and organic N sources (i.e., 1 mM Tris + 0.8 mM NH_3) impaired the growth of both strains (Bonferroni test, $p < 0.05$, Fig. 5C). At low N levels (i.e., 0.08 mM NH_3), UIB 001 responded better than 4B UA. However, organic N (i.e., 1 mM Tris) was more toxic to UIB 001 than 4B UA (Bonferroni test, $p < 0.05$, Fig. 5C).

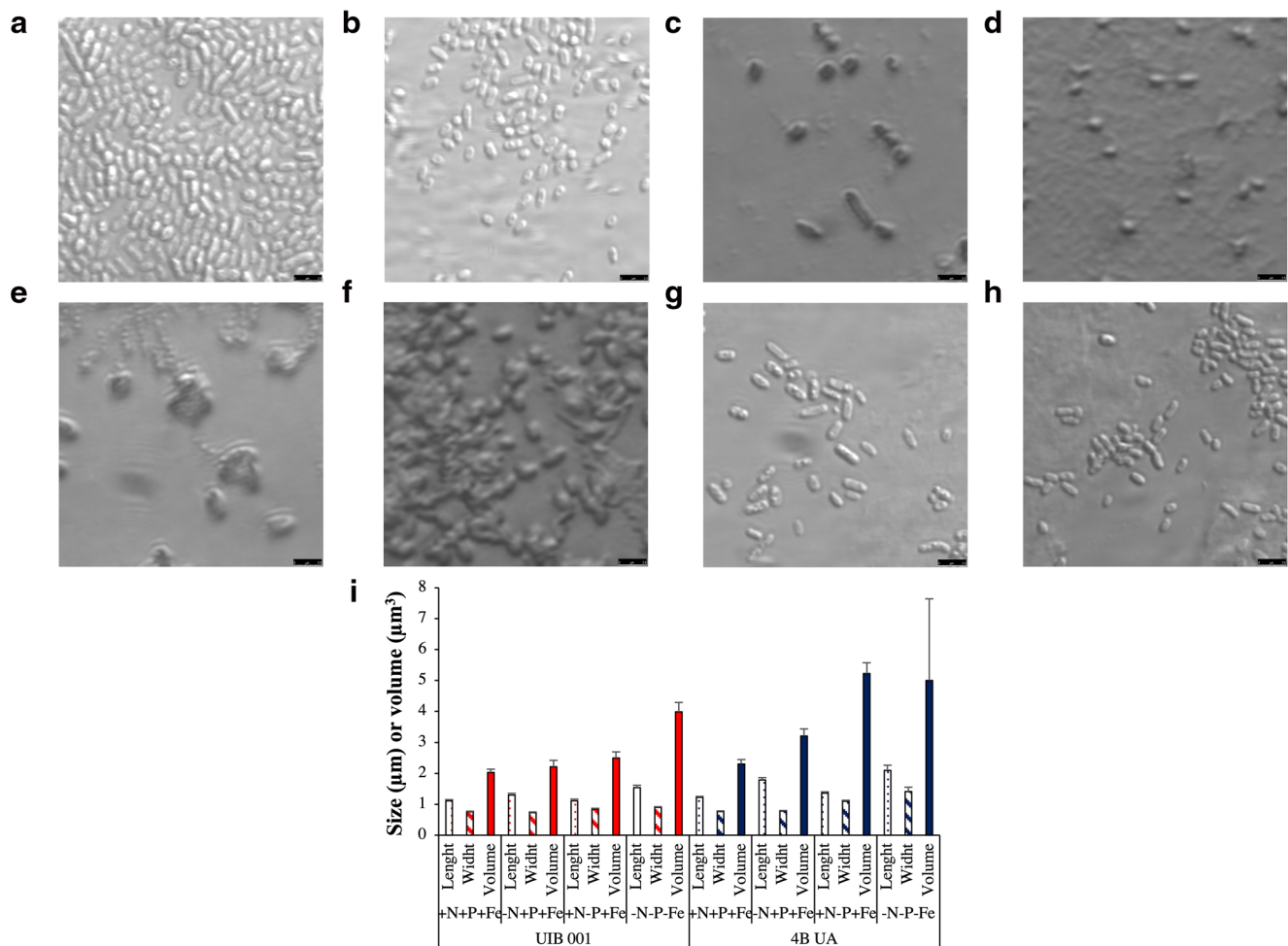


Fig. 4 Microscopic analysis of *Cobetia* sp. UIB 001 and 4B UA under different N, P, and Fe nutrient regimes. **A** Optimal condition, +N + P + Fe + C, for the UIB 001 strain. **B** Optimal condition, +N + P + Fe + C, for the 4B UA strain. **C** N_2 as the sole N source, -N + P + Fe + C, for the UIB 001 strain. **D** N_2 as the sole N source, -N + P + Fe + C, for the 4B UA strain. **E** P- and Fe-depleted condition, +N-P-Fe + C, for the UIB 001 strain. **F** P- and Fe-depleted condition, +N-P-Fe + C, for the 4B UA strain. **G** Nutrient-depleted condition, -N-P-Fe + C, for the UIB 001 strain. **H** Nutrient-depleted condition, -N-P-Fe + C, for the 4B UA strain. **I** Length, width, and volume changes derived from changes in nutrient regimes for *Cobetia* sp. UIB 001 and 4B UA. For **A-H**, microscopical images were taken at $\times 100$ with 4.73 of zoom

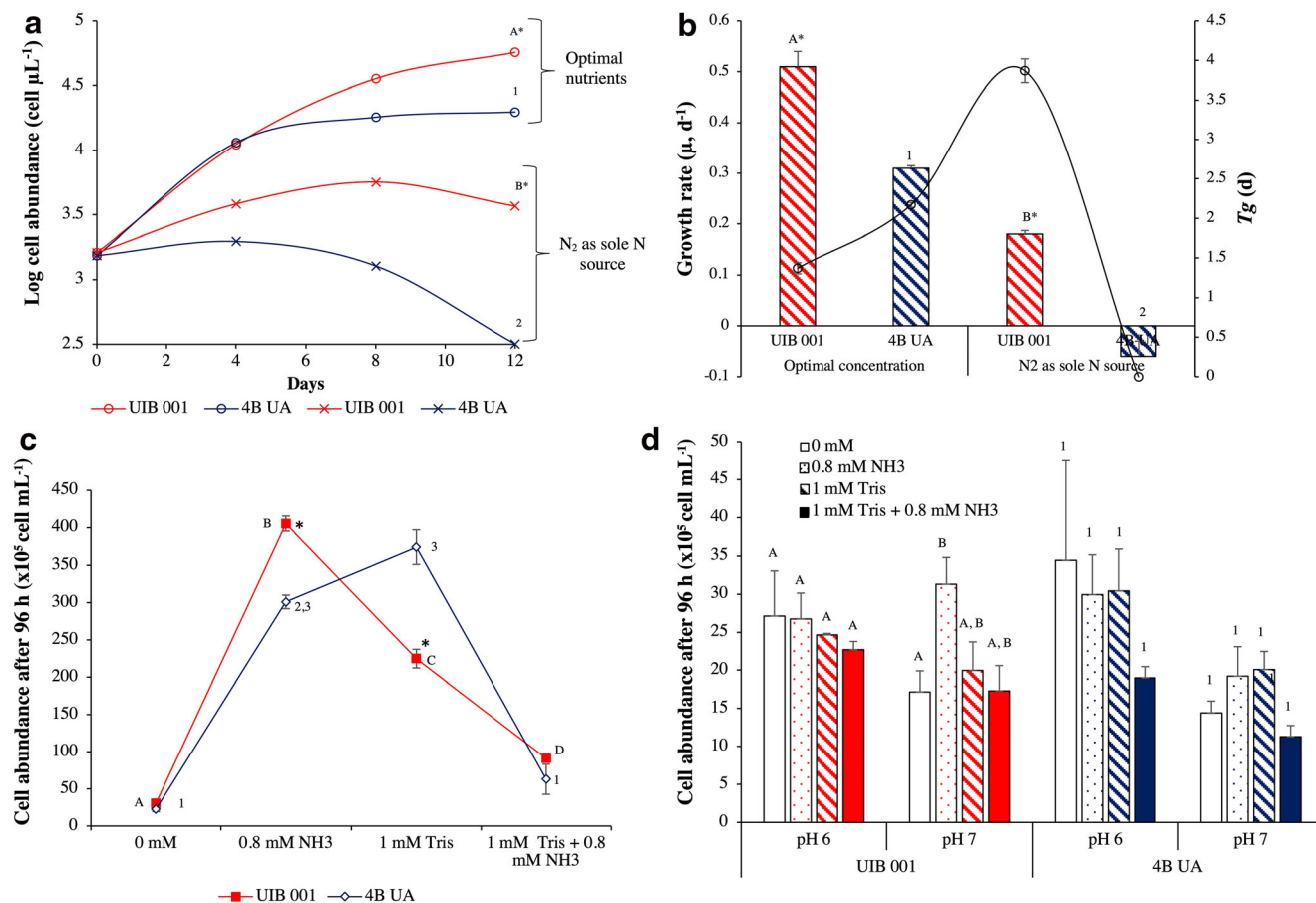


Fig. 5 Nitrogen (N) concentration effect for *Cobetia* sp. UIB 001 and 4B UA. **A–B** Long-term effect. **A** Growth curve under the optimal condition and **B** growth rate (μ , d^{-1} , as a bar chart) and duplication time (T_g , d, as a line) under the optimal condition and N_2 as the sole N source. **C–D** Short-term (cell abundance, $cell\ mL^{-1}$) after 96 h under different N sources (inorganic, NH_3 , or organic, Tris) at **C** pH 8 and

D at pH 6 and 7. Values are the mean \pm SE between the replicates. Letters (for UIB 001) and numbers (for 4B UA) indicate significant differences according to the treatment inside each strain, and asterisks (*) indicate significant differences between each strain inside each treatment, using a post hoc test (Bonferroni test, $p < 0.05$) after ANOVA over the whole dataset

Lowering pH to 6 or 7 affected growth to a higher degree than the N source itself (ANOVA, $p < 0.05$, Fig. 5D). Indeed, the significant differences found previously were banished when pH was dropped, without any differences between strains (ANOVA, $p > 0.05$, Fig. 5D), except for UIB 001 at pH 7, in which 0.8 mM of NH_3 had a positive impact on cell abundance (Bonferroni test, $p < 0.05$, Fig. 5D).

Changes of P and Fe Concentrations

Long-Term Effect of P and Fe Not surprisingly, higher growth rates (μ) were reached under optimal PO_4^{3-} and Fe concentrations than at low PO_4^{3-} , decreasing growth \approx 2-fold for both strains, and more pronouncedly at low Fe levels (ANOVA, $p < 0.05$, Fig. 6A and B). Noteworthy, higher μ and lower T_g were reached by UIB 001, compared to 4B UA, independently of the nutrient levels (Bonferroni test, $p < 0.05$, Fig. 6B).

Short-Term Effects of P and Fe Along with pH Short-term studies (during 96 h) showed that for both strains, PO_4^{3-} /Fe concentrations and pH levels (6, 7, and 8) variations significantly affected cell abundances (ANOVA, $p < 0.05$, Fig. 6C). Overall, low concentrations of PO_4^{3-} and Fe combined with different pH levels (6–8) did not significantly differ between strains (ANOVA, $p > 0.05$, Fig. 6C), albeit a higher tolerance to lower pH was observed for the UIB 001 strain. However, at pH 8 and low PO_4^{3-} and Fe levels, UIB 001 grew as it did at high PO_4^{3-} and Fe levels (Bonferroni test, $p > 0.05$, Fig. 6C), as opposed to 4B UA (Bonferroni test, $p < 0.05$, Fig. 6C). Decreasing pH levels had a dramatic effect on cell abundances (i.e., pH 6 and 7) (Bonferroni test, $p < 0.05$, Fig. 6C), showing that pH 8 was the optimum for UIB 001 and 4B UA strains independently of PO_4^{3-} and Fe levels (Fig. 6C).

Effect of Low Concentrations of P and Fe The responses to low PO_4^{3-} and Fe availability (under long term or short term) for both strains revealed an independent effect of P and Fe (P

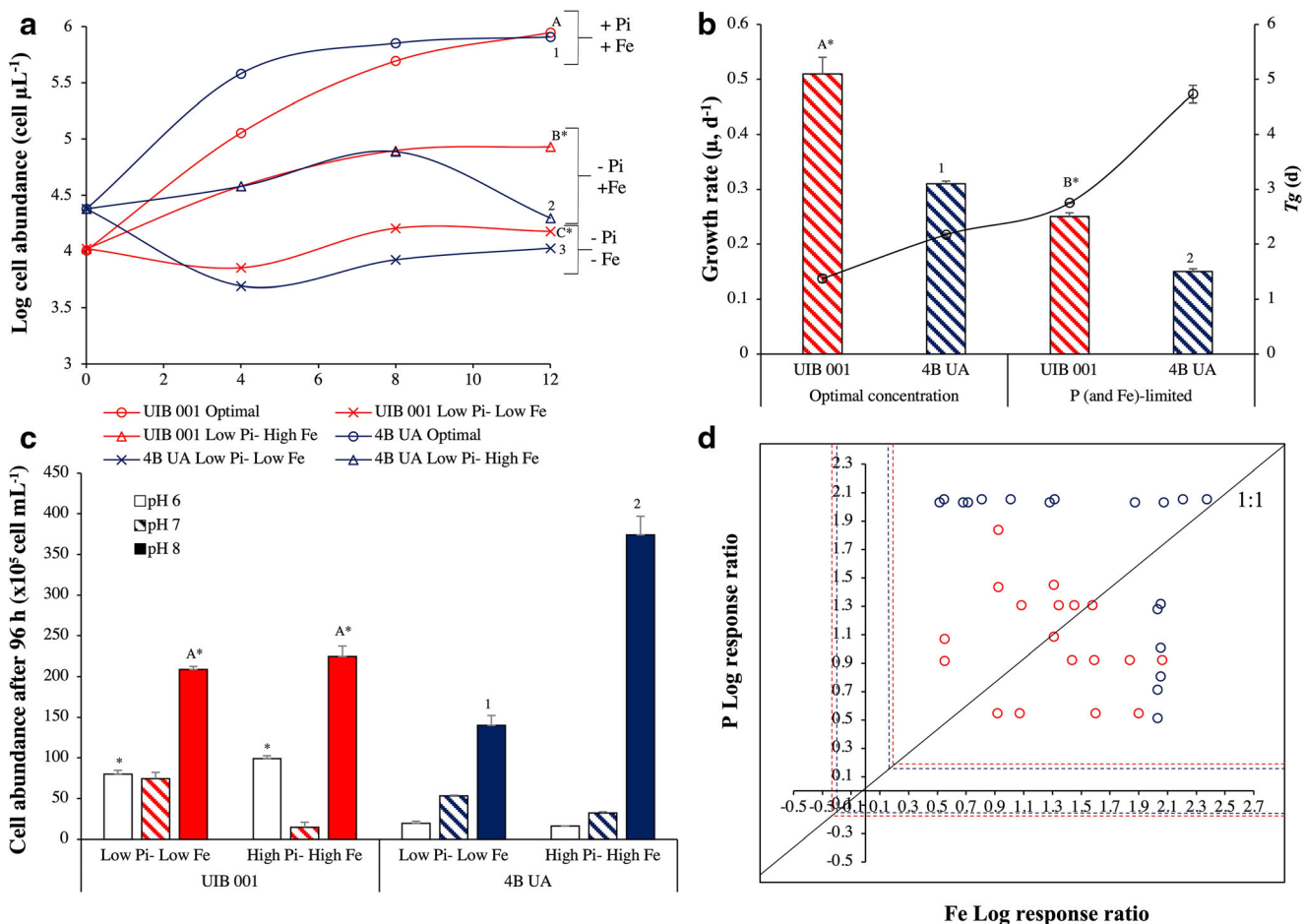


Fig. 6 Phosphorus (P) and Fe concentration effect for *Cobetia* sp. UIB 001 and 4B UA. **A–B** Long-term effect studies. **A** Growth curve under optimal nutrient condition and low PO_4^{3-} and/or Fe concentrations (0.005 μM and/or 1 nM, respectively) and **B** growth rate (μ, d^{-1} , as a bar chart) and duplication time (T_g, d , as a line) curve under optimal nutrient condition and low PO_4^{3-} and/or Fe concentrations. **C** Short-term studies (cell abundance, cell mL^{-1}) after 96 h under different PO_4^{3-} and Fe concentrations at pH 6, 7, and 8. In **A–C** values are the mean \pm SE between the replicates. Letters (for UIB 001) and numbers (for 4B UA) indicate significant differences according to the treatment inside

response >0 , Fe response >0 and P + Fe response >0 , $p < 0.05$, Fig. 6D). The threshold for P and Fe was slightly lower for UIB 001 than 4B UA, displaying a better response to low concentrations of P and Fe.

Effects of P on APA and Structure of PhoD The alkaline phosphatase activity (APA) was extremely influenced by pH at low PO_4^{3-} levels, i.e., 0.005 μM (ANOVA, $p < 0.05$, Fig. 7A). Alkaline pH (i.e., pH 8) enhanced APA an average of 40-fold in both strains compared with the acidify conditions (Bonferroni test, $p < 0.05$, Fig. 7A). Different Fe levels (1 nM–1 μM) did not cause any significant differences in APA at [Low PO_4^{3-}], i.e., 0.005 μM (ANOVA, $p < 0.05$, Fig. 7A). Increasing levels of PO_4^{3-} (up to 100 μM) induced different inhibition responses on each strain (ANOVA,

each strain, and asterisks (*) indicate significant differences between each strain inside each treatment, using a post hoc test (Bonferroni test, $p < 0.05$) after ANOVA over the whole dataset. PO_4^{3-} is represented as Pi. **D** Log P and Fe responses. Each data point represents each replicate (red: UIB 001; blue: 4B UA) in which X-axis is the P log response and Y-axis is the Fe log response. Dashed red (for *Cobetia* sp. UIB 001) and blue lines (*Cobetia* sp. 4B UA) represent the critical threshold values (data points outside the critical values are significantly different (at $p = 0.05$) from P_0Fe_0)

$p < 0.05$, Fig. 7B), detecting positive feedback with Fe, especially for the *Cobetia* sp. UIB 001 (Fig. 7B). For the UIB 001, at pH 8 and high levels of Fe (1 μM), APA did not respond to higher P levels (up to 50 μM) and required the highest PO_4^{3-} level (100 μM) to inhibit its activity (Bonferroni test, $p < 0.05$, Fig. 7B), unlike for 4B UA in which APA at 50 μM was significantly inhibited (Bonferroni test, $p < 0.05$, Fig. 7B).

Structural analysis revealed the potential protein structure and the catalytic center for both PhoD of UIB 001 and 4B UA (Fig. 7 C and D). PhoD sequences shared an identity of 88%, while at the structural level, they shared an identity of 76%. Both PhoD had the same catalytic center as predicted for the PhoD of *C. amphilecti* KMM 296 (WP_043333989): ASP (241/238), TYR (244/241), ASP (306/303), HIS (308/305),

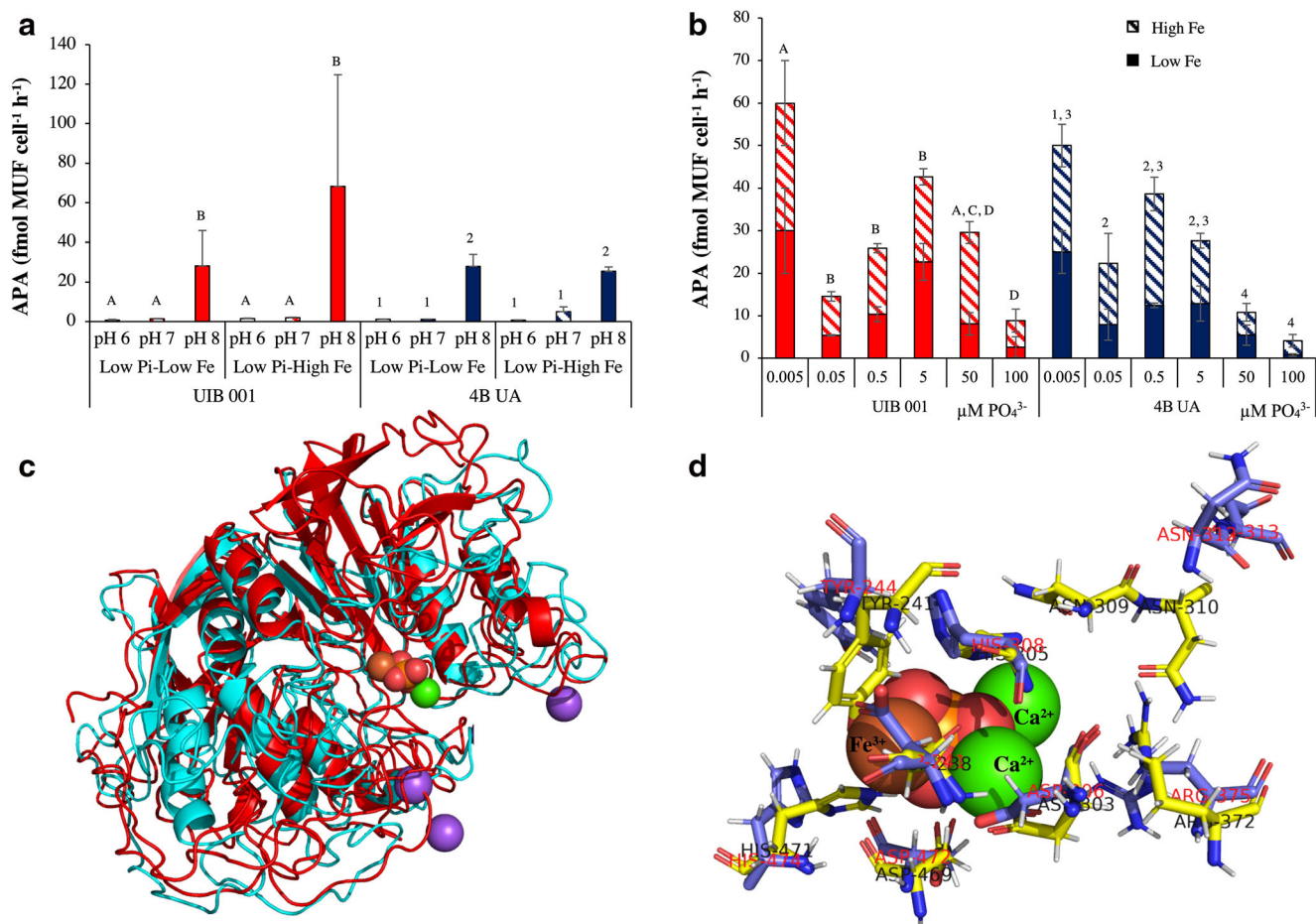


Fig. 7 P-acquisition mechanisms for *Cobetia* sp. UIB 001 and 4B UA. **A** Alkaline phosphatase activity (APA) under low levels of PO_4^{3-} (0.005 μM) and differential concentration of Fe (1 nM and 1 μM). **B** APA under different levels of PO_4^{3-} (0.005–100 μM). Solid bars are low Fe level conditions, whereas the striped bars are under high levels conditions. Values are the mean \pm SE between the replicates. Letters (for UIB 001) and numbers (for 4B UA) indicate significant differences

ASN (312/309), ASN (313/310), ARG (375/372), ASP (472/469), and HIS (474/471) (Fig. 7D).

Effects of N, P, and Fe on ROS Production Along with pH
Different pH levels had a significant effect on ROS production for both strains (ANOVA, $p < 0.05$, Fig. 8A). Alkaline pH (i.e., pH 8) reduced an average of 15-fold ROS compared with the acidify conditions (Bonferroni test, $p < 0.05$, Fig. 8A). At pH 8, ROS production was affected by the different sources of inorganic and organic N (ANOVA, $p < 0.05$, Fig. 8B). However, no significant differences were achieved between strains (ANOVA, $p > 0.05$, Fig. 8B), decreasing ROS production with an increase of N (ANOVA, $p < 0.05$, Fig. 8B). Indeed, different PO_4^{3-} and Fe levels did not have any effect on ROS production for both strains (ANOVA, $p > 0.05$, Fig. 8C), except for 4B UA at high concentrations of PO_4^{3-} and Fe, with ROS production decreasing significantly

according to the treatment inside each strain using a post hoc test (Bonferroni test, $p < 0.05$) after ANOVA over the whole dataset. PO_4^{3-} is represented as Pi. **C–D** Protein structural analysis base on the description of the PhoD of *C. amphilecti* KMM 296. **C** Structural analysis of PhoD from UIB 001 (red) and 4B UA (blue) strains. **D** Catalytic center for PhoD: UIB 001 strain, in red (aa letters) and blue (aa structure), and 4B UA, in black (aa letters) and yellow (aa structure)

compared to [Low PO_4^{3-} -High PO_4^{3-}] condition (Bonferroni test, $p < 0.05$, Fig. 8C).

Discussion

For decades, the study of microbial biodiversity has sought to determine why microbes live where they live, embracing the tenet that “Everything is everywhere, but the environment selects” [33]. Here, we isolate and identify two strains of the same species (i.e., as endophytic and epiphytic bacteria, *Cobetia* sp. UIB 001 and 4B UA) which thrive on two different seagrasses in contrasting environments: *Posidonia oceanica* found in the Mediterranean Sea (MS) and the *Heterozostera chilensis* (formerly *H. nigricaulis*) found in the Humboldt current system (HCS). As noticed before, the MS is an oligotrophic semi-enclosed sea, where *P. oceanica* is

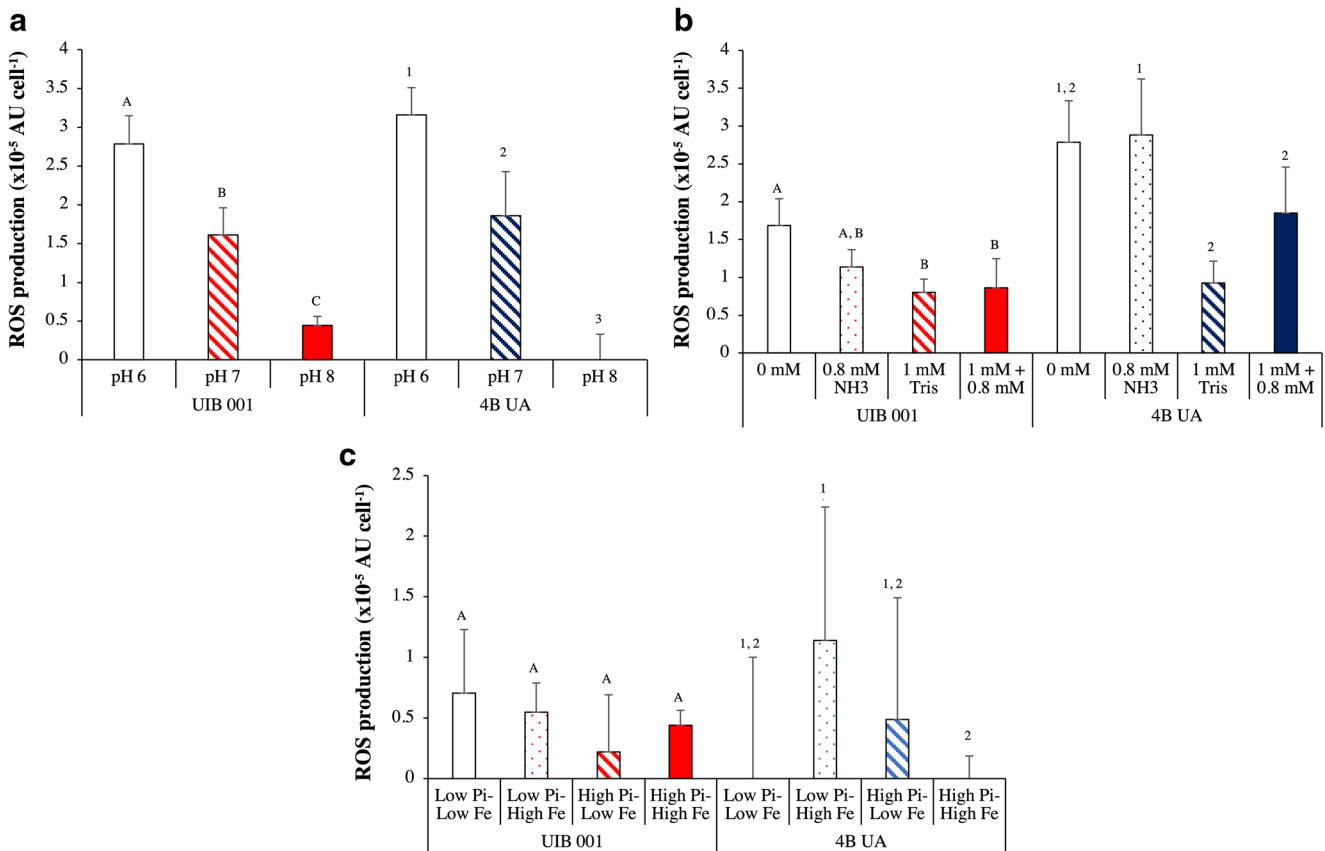


Fig. 8 Reactive oxygen production (ROS) production for *Cobetia* sp. UIB 001 and 4B UA. **A** At different pH levels (6–8). **B** At different concentrations of N source. **C** At different combinations of PO_4^{3-} and Fe. Values are the mean \pm SE between the replicates. Letters (for UIB

001) and numbers (for 4B UA) indicate significant differences according to the treatment inside each strain using a post hoc test (Bonferroni test, $p < 0.05$) after ANOVA over the whole dataset. PO_4^{3-} is represented as Pi

widely extended, while the HCS is a nutrient-rich cold current where *H. chilensis* thrives in just a few locations, settled relatively recently [21]. Our results suggest that regardless of the contrasting environments considered, the same endophytic and epiphytic bacteria can perform analogous functions and adapt similarly to stressful scenarios.

After culturing the whole epiphytic community of both seagrasses, the gamma-proteobacteria *Cobetia* sp. (UIB 001 and 4B UA) arose above all in both seagrasses. Although we made an effort to taxonomic classify these isolates, it was only possible to determine that both strains are the same *Cobetia* species, presumably *C. amphilecti*, and they do not belong to the *Cobetia marina* species. Due to the lack of type strain genome sequences of the genus *Cobetia*, precise taxonomic classifications cannot be performed from the genomic point of view. From a genomic view, high G + C % contents were detected in both strains (i.e., 62–63%), which has previously been correlated to N availability [65]. This means that the ecological niche of *Cobetia* sp. UIB 001 and 4B UA are rich in N, probably by the high rates of N_2 -fixation detected in *P. oceanica* (i.e., higher than the rest of tropical seagrasses) [9] and the high N availability in the HCS [19]. Even though

Balabanova et al. (2016ab) did not show physiological data, it revealed the potential genomic adaptation to the changing nutrient regimes of *C. amphilecti*, reporting different metabolic and biochemical profiles between differential strains placed in different marine niches [66, 67]. Yet, this work reveals that the *Cobetia* sp. isolates respond differently to seawater conditions. Thus, we hypothesize that these different traits might be the consequence of a different genomic evolution subjected to environmental pressures that led to the development of specific proteins and the significant number of SNPs that were found.

According to classical classifications [68, 69], both *Cobetia* sp. strains (UIB 001 and 4B UA), might belong to the group of oligotrophic bacteria, as they were capable of growing with minimal content of organic matter and nutrients (i.e., 1–15 mg of C mL⁻¹ and N_2 as the sole N source). Indeed, these strains may be considered as extreme oligotrophic bacteria, as they were able to grow with N_2 as the sole N source, and P- and Fe-depleted conditions, being just dependent on the carbon (C) source (e.g., citrate or glucose), as metabolic tests revealed. Oligotrophic bacteria usually have small sizes ($\leq 1 \mu\text{m}$) to optimize the low availability of resources

available by increasing their S/V ratio. However, microbes can expand their size to increase the cell surface area to accommodate enough uptake sites to meet uptake demands [70], as observed in both *Cobetia* sp. Through this plasticity to respond to the changing environment, bacteria play a key role in marine food webs and nutrient recycling (e.g., accumulation, export, remineralization, and transformation of nutrients), being a reservoir for nutrients as C, N, and P [71, 72], as *Cobetia* sp. does for the sustenance and maintenance of both seagrasses.

The ability to grow with N₂ as the sole N source and the N₂-fixation activity found in the UIB 001, remarks its potential role as N₂-fixer, as previously seen in other *Cobetia* spp., isolated as hydrocarbon-utilizing microbiota [73, 74]. Although non-putative N₂-fixation genes annotated were found in their genomes (i.e., UIB 001 and 4B UA), genes typically involved in N₂-fixing bacteria as ADP-ribosyl (dinitrogen reductase) glycohydrolase (*draG*), which products can regulate the nitrogenase complex (i.e., formed by NifH, NifK, and NifD) [75], and *cbb3*-type cytochrome c oxidase, required for symbiotic N₂-fixation [76], were found in both bacteria. This observation may suggest that the UIB 001 might contain alternative genes for N₂-fixation. Noteworthy, the utilization of trace amounts of atmospheric ammonia through high-affinity ammonium transporters (AmtB) might be also a potential source of N for extreme oligotrophic bacteria [77], which explains why isolated 4B UA was capable of growth in (semi)solid media with N₂ as sole N source.

In vast oligotrophic areas of the ocean, N₂-fixation is limited by P [78], while, in eutrophic coastal areas, P can trigger harmful algal blooms [79]. In our experiments, only the 4B UA strain isolated from the eutrophic HCS was P limited, as opposed to the oligotrophic MS isolate (UIB 001) that was relatively unaffected. Contrariwise, APA of the UIB 001 strain was prolonged with a higher concentration of PO₄³⁻ (without enhancing ROS production, unlike the 4B UA), suggesting a higher P-demand to achieve homeostasis. Previously, it was observed that under low concentrations of P, bacteria associated with *P. oceanica* (e.g., *Halotheca* sp. species) were able to release dissolved inorganic phosphorus (DIP) from dissolved organic phosphorus (DOP) through the alkaline phosphatases (APases), which are expressed and activated through the PhoB-PhoR system [30]. Alkaline phosphatase D (PhoD) varied between the two strains at the sequence and structural levels, 88% and 76%, respectively, pointing to the structural differences as the most relevant in the differential APA, due to the lack of differences at the catalytic center.

Both APases are Fe-dependent (such as antioxidant enzymes or the nitrogenase complex [27, 80]) and are therefore impacted by the extended iron limitation throughout the ocean, including the MS and the HCS [17]. For both strains, APA was enhanced by increasing Fe levels since we predict in

our PhoD model the coordination with one Fe³⁺ atom. However, high Fe levels did not induce ROS production at the optimal pH 8. Ferric iron, Fe³⁺, is insoluble at neutral pH, but at a lower pH, its solubility increases. At acidified pH, organic ligands have less affinity for Fe, reducing Fe absorption and thus affecting cell growth [81]. Moreover, ROS production was enhanced under acidic pH (i.e., pH 6), possibly by lower intracellular Fe content for antioxidant enzymes (e.g., superoxide dismutase, catalase, glutathione reductase, or glutathione peroxidase).

The increasing carbon dioxide (CO₂) concentrations emitted to the atmosphere are irremissibly increasing ocean acidification (OA), posing serious risks to marine life [82]. However, lower pH levels may ameliorate some of the concomitant impacts of OA, i.e., reducing the impacts of un-ionized NH₃ on the activity of some cytosolic enzymes [83]. Both *Cobetia* sp. were significantly affected by high N sources at pH 8, but not at pH 6 or 7, not accompanied by ROS increments, suggesting that antioxidant enzymes were not affected by un-ionized NH₃. Moreover, it has been observed that OA may play a significant role in P eutrophication [84]. Previous works pointed to the sensitivity of the APA of *Cobetia* spp. exposed to acidification [61, 85, 86].

Our multifactorial design showed that the same species growing in different ocean basins (i.e., MS or HCS) displays different physiological and biochemical responses to different nutrient regimes (N, P, and/or Fe). Not surprisingly, the Mediterranean strain (exposed to oligotrophic water of the MS) coped with low N and P concentrations more efficiently. Nonetheless, the appearance of oligotrophic bacteria in nutrient replete waters (i.e., 4B UA) may point to the origin of this species, as its host, *H. chilensis*, reached the Chilean coast after long-distance dispersal from its native East Australian Current [21], characterized by warm waters and oligotrophy. Moreover, this species settled ~30°S, where a drop in primary production has been associated with the poleward migration of the South Pacific Anticyclone [87], pointing to substrate availability as the more important factor controlling bacterial activity and abundance in the HCS [88].

Conclusions

In summary, the present study brings new clues to better understand how biotic (host) and abiotic (i.e., nutrient levels and pH) interactions affect the plasticity and phenotypic acclimation of epiphytic bacteria thriving in contrasting environments, pointing to the intriguing relationships between epiphytes and seagrasses on the nutrients cycling around the global ocean.

Supplementary Information The online version contains supplementary material available at <https://doi.org/10.1007/s00248-021-01766-z>.

Acknowledgements VFJ acknowledges the travel funds provided by the Santander Iberoamérica 2019–2020 fellowship. We are grateful to Prof. Mario Edding and Felipe Sáez of the Laboratorio de Botánica Marina at the Universidad Católica del Norte for providing us with leaves of *H. chilensis*.

Author Contribution VFJ and PE designed the experiments. VFJ conducted all the laboratory experiments and isolated the UIB 001 strain. JBE isolated the Pacific 4B UA strain. DJL conducted the bioinformatic analyses. All the authors, VFJ, DJL, JBE, ABF, NSRA, and PE, led the writing of the paper.

Funding NSRA was funded through the Ministerio de Economía, Industria y Competitividad-Agencia Estatal de Investigación and the European Regional Development Funds project (CTM2016-75457-P). PE acknowledges the financial support of the research grants Fondecyt Iniciación 11170837, FONDEQUIP EQM120137, and REDII70403.

Data and Availability and Code Availability This manuscript contains previously unpublished data. The name of the repository and accession number(s) are CP058244 to CP058245 (*Cobetia* sp. UIB 001) and CP059843 to CP059845 (*Cobetia* sp. 4B UA).

Declarations

Studies Involving Animal Subjects No animal studies are presented in this manuscript.

Studies Involving Human Subjects No human studies are presented in this manuscript.

Inclusion of Identifiable Human Data No potentially identifiable human images or data is presented in this study.

Consent to Participate Not applicable.

Consent for Publication Not applicable.

Conflict of Interest The authors declare no competing interests.

References

- Hemminga MA, Duarte CM (2002) Seagrass ecology. Cambridge University Press. James W. Fourqurean. <https://doi.org/10.4319/lo.2002.47.2.0611>
- Gutiérrez JL, Jones CG, Byers JE, Arkema KK, Berkenbusch K, Commito A et al (2012) Physical ecosystem engineers and the functioning of estuaries and coasts. *Treatise Estuar Coast Sci* 7: 58–81. <https://doi.org/10.1016/B978-0-12-374711-2.00705-1>
- Renn CE (1937) Bacteria and the phosphorus cycle in the sea. *Biol Bull* 72:190–195
- Tortell PD, Maldonado MT, Price NM (1996) The role of heterotrophic bacteria in iron-limited ocean ecosystems. *Nature*. 383:330–332. <https://doi.org/10.1038/383330a0>
- Anderson OR (2018) Evidence for coupling of the carbon and phosphorus biogeochemical cycles in freshwater microbial communities. *Front Mar Sci* 5:1–6. <https://doi.org/10.3389/fmars.2018.00020>
- Flombaum P, Gallegos JL, Gordillo RA, Rincon J, Zabala LL, Jiao N, Karl DM, Li WKW, Lomas MW, Veneziano D, Vera CS, Vrugt JA, Martiny AC (2013) Present and future global distributions of the marine Cyanobacteria *Prochlorococcus* and *Synechococcus*. *Proc Natl Acad Sci* 110:9824–9829. <https://doi.org/10.1073/pnas.1307701110>
- Ugarelli K, Chakrabarti S, Laas P, Stingl U (2017) The seagrass holobiont and its microbiome. *Microorganisms* 5:81. <https://doi.org/10.3390/microorganisms5040081>
- Sohm JA, Webb EA, Capone DG (2011) Emerging patterns of marine nitrogen fixation. *Nat Rev Microbiol* 9:499–508. <https://doi.org/10.1038/nrmicro2594>
- Agawin NSR, Ferriol P, Cryer C, Alcon E, Busquets A, Sintes E, Vidal C, Moyà G (2016) Significant nitrogen fixation activity associated with the phyllosphere of Mediterranean seagrass *Posidonia oceanica*: first report. *Mar Ecol Prog Ser* 551:53–62. <https://doi.org/10.3354/meps11755>
- Agawin NSR, Ferriol P, Sintes E, Moyà G (2017) Temporal and spatial variability of in situ nitrogen fixation activities associated with the Mediterranean seagrass *Posidonia oceanica* meadows. *Limnol Oceanogr* 62:2575–2592. <https://doi.org/10.1002/lno.10591>
- Agawin NSR, Ferriol P, Sintes E (2019) Simultaneous measurements of nitrogen fixation activities associated with different plant tissues of the seagrass *Posidonia oceanica*. *Mar Ecol Prog Ser* 611: 111–127. <https://doi.org/10.3354/meps12854>
- Perry CJ, Dennison WC (1999) Microbial nutrient cycling in seagrass sediment. *J Aust Geol Geophys* 17:227–231
- Tanhua T, Hainbucher D, Schroeder K, Cardin V, Álvarez M, Civitarese G (2013) The Mediterranean Sea system: a review and an introduction to the special issue. *Ocean Sci* 9:789–803. <https://doi.org/10.5194/os-9-789-2013>
- Thingstad TF, Krom MD, Mantoura RFC, Flaten GA, Groom S, Herut B, Kress N, Law CS, Pasternak A, Pitta P, Psarra S, Rassoulzadegan F, Tanaka T, Tselepides A, Wassmann P, Woodward EM, Riser CW, Zodiatis G, Zohary T (2005) Nature of phosphorus limitation in the ultraoligotrophic eastern Mediterranean. *Science* (80-) 309:1068–1071. <https://doi.org/10.1126/science.1112632>
- Ridame C, Le Moal M, Guieu C et al (2011) Nutrient control of N₂ fixation in the oligotrophic Mediterranean Sea and the impact of Saharan dust events. *Biogeosciences* 8:2773–2783. <https://doi.org/10.5194/bg-8-2773-2011>
- Statham PJ, Hart V (2005) Dissolved iron in the Cretan Sea (eastern Mediterranean). *Limnol Oceanogr* 50:1142–1148. <https://doi.org/10.4319/lo.2005.50.4.1142>
- Moore JK, Doney SC, Glover DM, Fung IY (2001) Iron cycling and nutrient-limitation patterns in surface waters of the world ocean. *Deep Res Part II Top Stud Oceanogr* 49:463–507. [https://doi.org/10.1016/S0967-0645\(01\)00109-6](https://doi.org/10.1016/S0967-0645(01)00109-6)
- Thiel M, Macaya EC, Acuña E, Amtz WE, Bastias H, Brokordt K, Camus PA, Castilla JC, Castro LR, Cortés M, Dumont CP, Escribano R, Fernández M, Gajardo JA, Gaymer CF, Gomez I, González AE, González HE, Haye PA et al (2007) The Humboldt Current System of Northern and Central Chile oceanographic processes, ecological interactions and socioeconomic feedback. *Oceanogr Mar Biol* 195–344
- Montecino V, Lange CB (2009) The Humboldt Current System: ecosystem components and processes, fisheries, and sediment studies. *Prog Oceanogr* 83:65–79. <https://doi.org/10.1016/j.pocean.2009.07.041>
- Kuo J (2005) A revision of the genus *Heterozostera* (*Zosteraceae*). *Aquat Bot* 81:97–140. <https://doi.org/10.1016/j.aquabot.2004.10.005>

21. Smith TM, York PH, Broitman BR, Thiel M, Hays GC, van Sebille E, Putman NF, Macreadie PI, Sherman CDH (2018) Rare long-distance dispersal of a marine angiosperm across the Pacific Ocean. *Glob Ecol Biogeogr* 27:487–496. <https://doi.org/10.1111/geb.12713>
22. Santelices B (1980) Phytogeographic characterization of the temperate coast of Pacific South America. *Phycologia*. 19:1–12. <https://doi.org/10.2216/i0031-8884-19-1-1.1>
23. Mahowald NM, Hamilton DS, Mackey KRM, Moore JK, Baker AR, Scanza RA, Zhang Y (2018) Aerosol trace metal leaching and impacts on marine microorganisms. *Nat Commun* 9:2614. <https://doi.org/10.1038/s41467-018-04970-7>
24. Moore CM, Mills MM, Arrigo KR, Berman-Frank I, Bopp L, Boyd PW, Galbraith ED, Geider RJ, Guieu C, Jaccard SL, Jickells TD, la Roche J, Lenton TM, Mahowald NM, Marañón E, Marinov I, Moore JK, Nakatsuka T, Oschlies A, Saito MA, Thingstad TF, Tsuda A, Ulloa O (2013) Processes and patterns of oceanic nutrient limitation. *Nat Geosci* 6:701–710. <https://doi.org/10.1038/ngeo1765>
25. Bristow LA, Mohr W, Ahmerkamp S, Kuypers MMM (2017) Nutrients that limit growth in the ocean. *Curr Biol* 27:R474–R478. <https://doi.org/10.1016/j.cub.2017.03.030>
26. Sebastian M, Ammerman JW (2011) Role of the phosphatase PhoX in the phosphorus metabolism of the marine bacterium *Ruegeria pomeroyi* DSS-3. *Environ Microbiol Rep* 3:535–542. <https://doi.org/10.1111/j.1758-2229.2011.00253.x>
27. Lesser MP (2006) Oxidative stress in marine environments: biochemistry and physiological ecology. *Annu Rev Physiol* 68:253–278
28. Yang M, Zhao W, Xie X (2014) Effects of nitrogen, phosphorus, iron and silicon on growth of five species of marine benthic diatoms. *Acta Ecol Sin* 34:311–319. <https://doi.org/10.1016/j.chnaes.2014.10.003>
29. Garcia NS, Fu F, Sedwick PN, Hutchins DA (2015) Iron deficiency increases growth and nitrogen-fixation rates of phosphorus-deficient marine cyanobacteria. *ISME J* 9:238–245. <https://doi.org/10.1038/ismej.2014.104>
30. Fernández-Juárez V, Bennasar-Figueras A, Tovar-Sanchez A, Agawin NSR (2019) The role of iron in the P-acquisition mechanisms of the unicellular N₂-fixing cyanobacteria *Halothece* sp., found in association with the Mediterranean seagrass *Posidonia oceanica*. *Front Microbiol* 10. <https://doi.org/10.3389/fmicb.2019.01903>
31. Fernández-Juárez V, Bennasar-Figueras A, Sureda-Gomila A, Ramis-Munar G, Agawin NSR (2020) Differential effects of varying concentrations of phosphorus, iron, and nitrogen in N₂-fixing cyanobacteria. *Front Microbiol* 11. <https://doi.org/10.3389/fmicb.2020.541558>
32. Browning TJ, Achterberg EP, Yong JC, Rapp I, Utermann C, Engel A, Moore CM (2017) Iron limitation of microbial phosphorus acquisition in the tropical North Atlantic. *Nat Commun* 8:1–7. <https://doi.org/10.1038/ncomms15465>
33. Baas-Becking LGM (1934) Geobiologie of inleiding tot de milieukunde. W.P. Van Stockum & Zoon, The Hague, the Netherlands
34. Sanz-Sáez I, Salazar G, Sánchez P, Lara E, Royo-Llonch M, Sà EL, Lucena T, Pujalte MJ, Vaqué D, Duarte CM, Gasol JM, Pedrós-Alió C, Sánchez O, Acinas SG (2020) Diversity and distribution of marine heterotrophic bacteria from a large culture collection. *BMC Microbiol* 20:1–16. <https://doi.org/10.1186/s12866-020-01884-7>
35. Arahall DR, Ventosa A (2006) The family *Halomonadaceae*. In: E S (ed) *The Prokaryotes*. Springer, New York, pp 811–835
36. De La Haba RR, Arahall DR, Márquez MC, Ventosa A (2010) Phylogenetic relationships within the family *Halomonadaceae* based on comparative 23S and 16S rRNA gene sequence analysis. *Int J Syst Evol Microbiol* 60:737–748. <https://doi.org/10.1099/ijs.0.013979-0>
37. Romanenko LA, Tanaka N, Svetashev VI, Falsen E (2013) Description of *Cobetia amphilecti* sp. nov., *Cobetia litoralis* sp. nov. and *Cobetia pacifica* sp. nov., classification of Halomonas halodurans as a later heterotypic synonym of *Cobetia marina* and emended descriptions of the genus *Cobetia* and *Cobetia marina*. *Int J Syst Evol Microbiol* 63:288–297. <https://doi.org/10.1099/ijs.0.036863-0>
38. Kim MS, Roh SW, Bae JW (2010) *Cobetia crustatorum* sp. nov., a novel slightly halophilic bacterium isolated from traditional fermented seafood in Korea. *Int J Syst Evol Microbiol* 60:620–626. <https://doi.org/10.1099/ijs.0.008847-0>
39. Arahall DR, Castillo AM, Ludwig W, Schleifer KH, Ventosa A (2002) Proposal of *Cobetia marina* gen. nov., comb. nov., within the family *Halomonadaceae*, to include the species *Halomonas marina*. *Syst Appl Microbiol* 25:207–211. <https://doi.org/10.1078/0723-2020-00113>
40. Yumoto I, Hirota K, Iwata H, Akutsu M, Kusumoto K, Morita N, Ezura Y, Okuyama H, Matsuyama H (2004) Temperature and nutrient availability control growth rate and fatty acid composition of facultatively psychrophilic *Cobetia marina* strain L-2. *Arch Microbiol* 181:345–351. <https://doi.org/10.1007/s00203-004-0662-8>
41. Ivanova EP, Christen R, Sawabe T, Alexeeva YV, Lysenko AM, Chelomin VP, Mikhailov VV (2005) Presence of ecophysiological diverse populations within *Cobetia marina* strains isolated from marine invertebrate, algae and the environments. *Microbes Environ* 20:200–207. <https://doi.org/10.1264/jsm.2.20.200>
42. Ibacache-Quiroga C, Ojeda J, Espinoza-Vergara G, Olivero P, Cuellar M, Dinamarca MA (2013) The hydrocarbon-degrading marine bacterium *Cobetia* sp. strain MM1IDA2H-1 produces a biosurfactant that interferes with quorum sensing of fish pathogens by signal hijacking. *Microb Biotechnol* 6:394–405. <https://doi.org/10.1111/1751-7915.12016>
43. Lv N, Pan L, Zhang J, Li Y, Zhang M (2019) A novel microorganism for removing excess ammonia-N in seawater ponds and the effect of *Cobetia amphilecti* on the growth and immune parameters of *Litopenaeus vannamei*. *J World Aquacult Soc* 50:448–459. <https://doi.org/10.1111/jwas.12561>
44. Fernández-Juárez V, López-alforja X, Frank-comas A, Echeveste P (2021) “The good, the bad and the double-sword” effects of microplastics and their organic additives in marine bacteria. *Front Microbiol* 11:1–12. <https://doi.org/10.3389/fmicb.2020.581118>
45. Salvà Serra F, Salvà-Serra F, Svensson-Stadler L, Busquets A, Jaén-Luchoro D, Karlsson R, B. Moore E, Gomila M (2018) A protocol for extraction and purification of high-quality and quantity bacterial DNA applicable for genome sequencing: a modified version of the Marmur procedure. *Protoc Exch*. <https://doi.org/10.1038/protex.2018.084>
46. Wick RR, Judd LM, Gorrie CL, Holt KE (2017) Unicycler: resolving bacterial genome assemblies from short and long sequencing reads. *PLoS Comput Biol* 13:e1005595. <https://doi.org/10.1371/journal.pcbi.1005595>
47. Gurevich A, Saveliev V, Vyahhi N, Tesler G (2013) QUAST: quality assessment tool for genome assemblies. *Bioinformatics*. 29: 1072–1075. <https://doi.org/10.1093/bioinformatics/btt086>
48. Tatusova T, Dicuccio M, Badretdin A et al (2016) NCBI prokaryotic genome annotation pipeline. *Nucleic Acids Res* 44:6614–6624. <https://doi.org/10.1093/nar/gkw569>
49. Haft DH, DiCuccio M, Badretdin A, Brover V, Chetvermin V, O’Neill K, Li W, Chitsaz F, Derbyshire MK, Gonzales NR, Gwadz M, Lu F, Marchler GH, Song JS, Thanki N, Yamashita RA, Zheng C, Thibaud-Nissen F, Geer LY, Marchler-Bauer A, Pruitt KD (2018) RefSeq: an update on prokaryotic genome

- annotation and curation. *Nucleic Acids Res* 46:D851–D860. <https://doi.org/10.1093/nar/gkx1068>
50. Yoon SH, Ha SM, Kwon S, Lim J, Kim Y, Seo H, Chun J (2017) Introducing EzBioCloud: a taxonomically united database of 16S rRNA gene sequences and whole-genome assemblies. *Int J Syst Evol Microbiol* 67:1613–1617. <https://doi.org/10.1099/ijsem.0.001755>
 51. Kumar S, Stecher G, Tamura K (2016) MEGA7: molecular evolutionary genetics analysis version 7.0 for bigger datasets. *Mol Biol Evol* 33:1870–1874. <https://doi.org/10.1093/molbev/msw054>
 52. Richter M, Rosselló-Móra R, Oliver Glöckner F, Peplies J (2016) JSpeciesWS: a web server for prokaryotic species circumscription based on pairwise genome comparison. *Bioinformatics*. 32:929–931. <https://doi.org/10.1093/bioinformatics/btv681>
 53. Meier-Kolthoff JP, Auch AF, Klenk HP, Göker M (2013) Genome sequence-based species delimitation with confidence intervals and improved distance functions. *BMC Bioinformatics* 14:60. <https://doi.org/10.1186/1471-2105-14-60>
 54. Jaén-Luchoro D, Gonzales-Siles L, Karlsson R, Svensson-Stadler L, Molin K, Cardew S, Jense-Markopolous S, Ohlén M, Inganäs E, Skovbjerg S, Tindall BJ, Moore ERB (2020) *Corynebacterium sanguinis* sp. nov., a clinical and environmental associated corynebacterium. *Syst Appl Microbiol* 43:126039. <https://doi.org/10.1016/j.syapm.2019.126039>
 55. Contreras-Moreira B, Vinuesa P (2013) GET_HOMOLOGUES, a versatile software package for scalable and robust microbial pangenome analysis. *Appl Environ Microbiol* 79:7696–7701. <https://doi.org/10.1128/aem.02411-13>
 56. Huerta-Cepas J, Szklarczyk D, Heller D, Hernández-Plaza A, Forslund SK, Cook H, Mende DR, Letunic I, Rattei T, Jensen LJ, von Mering C, Bork P (2018) eggNOG 5.0: a hierarchical, functionally and phylogenetically annotated orthology resource based on 5090 organisms and 2502 viruses. *Nucleic Acids Res* 47:309–314. <https://doi.org/10.1093/nar/gky1085>
 57. Hillebrand H, Dürselen CD, Kirschtel D, Pollinger U, Zohary T (1999) Biovolume calculation for pelagic and benthic microalgae. *J Phycol* 35:403–424. <https://doi.org/10.1046/j.1529-8817.1999.3520403.x>
 58. Zhang Y (2008) I-TASSER server for protein 3D structure prediction. *BMC Bioinformatics* 9:40. <https://doi.org/10.1186/1471-2105-9-40>
 59. Finn RD, Coghill P, Eberhardt RY, Eddy SR, Mistry J, Mitchell AL, Potter SC, Punta M, Qureshi M, Sangrador-Vegas A, Salazar GA, Tate J, Bateman A (2016) The Pfam protein families database: towards a more sustainable future. *Nucleic Acids Res* 44:D279–D285. <https://doi.org/10.1093/nar/gkv1344>
 60. Li Z, Natarajan P, Ye Y, Hrade T, Godzik A (2014) POSA: a user-driven, interactive multiple protein structure alignment server. *Nucleic Acids Res* 42:W240–W245. <https://doi.org/10.1093/nar/gku394>
 61. Noskova Y, Likhatskaya G, Terentjeva N, Son O, Tekutyeva L, Balabanova L (2019) A novel alkaline phosphatase/phosphodiesterase, CamPhoD, from marine bacterium *Cobetia amphilecti* KMM 296. *Mar Drugs* 17:1–20. <https://doi.org/10.3390/md17120657>
 62. The UniProt Consortium (2014) UniProt: a hub for protein information. *Nucleic Acids Res* 43:D204–D212. <https://doi.org/10.1093/nar/gku989>
 63. DeLano WL (2002) The PyMOL molecular graphics system. Schrödinger, LLC. Available online at: <http://www.pymol.org>
 64. Park M, Kim C, Yang J, Lee H, Shin W, Kim S, Sa T (2005) Isolation and characterization of diazotrophic growth promoting bacteria from rhizosphere of agricultural crops of Korea. *Microbiol Res* 160:127–133. <https://doi.org/10.1016/j.micres.2004.10.003>
 65. Hellweger FL, Huang Y, Luo H (2018) Carbon limitation drives GC content evolution of a marine bacterium in an individual-based genome-scale model. *ISME J* 12:1180–1187. <https://doi.org/10.1038/s41396-017-0023-7>
 66. Balabanova LA, Golotin VA, Kovalchuk SN, Babii AV, Shevchenko LS, Son OM, Kosovsky GY, Rasskazov VA (2016) The genome of the marine bacterium *Cobetia marina* KMM 296 isolated from the mussel *Crenomytilus grayanus* (dunker, 1853). *Russ J Mar Biol* 42:106–109. <https://doi.org/10.1134/S106307401601003X>
 67. Balabanova L, Nedashkovskaya O, Podvolotskaya A, Slepchenko L, Golotin V, Belik A, Shevchenko L, Son O, Rasskazov V (2016) Data supporting functional diversity of the marine bacterium *Cobetia amphilecti* KMM 296. *Data Br* 8:726–732. <https://doi.org/10.1016/j.dib.2016.06.034>
 68. Kuznetsov SI, Dubinina GA, Lapteva NA (1979) Biology of oligotrophic bacteria. *Annu Rev Microbiol* 33:377–387. <https://doi.org/10.1146/annurev.mi.33.100179.002113>
 69. Schut F, Prins RA, Gottschal JC (1997) Oligotrophy and pelagic marine bacteria: facts and fiction. *Aquat Microb Ecol* 12:177–202
 70. Dao MH (2013) Reassessment of the cell surface area limitation to nutrient uptake in phytoplankton. *Mar Ecol Prog Ser* 489:87–92. <https://doi.org/10.3354/meps10434>
 71. Cole J, Findlay S, Pace M (1988) Bacterial production in fresh and saltwater ecosystems: a cross-system overview. *Mar Ecol Prog Ser* 43:1–10. <https://doi.org/10.3354/meps043001>
 72. Biddanda B, Ogdahl M, Cotner J (2001) Dominance of bacterial metabolism in oligotrophic relative to eutrophic waters. *Limnol Oceanogr* 46:730–739. <https://doi.org/10.4319/lo.2001.46.3.0730>
 73. Radwan S, Mahmoud H, Khanafer M, al-Habib A, al-Hasan R (2010) Identities of epilithic hydrocarbon-utilizing diazotrophic bacteria from the Arabian gulf coasts, and their potential for oil bioremediation without nitrogen supplementation. *Microb Ecol* 60:354–363. <https://doi.org/10.1007/s00248-010-9702-x>
 74. Al-Awadhi H, Al-Mailem D, Dashti N et al (2012) Indigenous hydrocarbon-utilizing bacterioflora in oil-polluted habitats in Kuwait, two decades after the greatest man-made oil spill. *Arch Microbiol* 194:689–705. <https://doi.org/10.1007/s00203-012-0800-7>
 75. Zhang Y, Burris RH, Ludden PW, Roberts GP (1997) Regulation of nitrogen fixation in *Azospirillum brasilense*. *FEMS Microbiol Lett* 152:195–204. [https://doi.org/10.1016/S0378-1097\(97\)00187-0](https://doi.org/10.1016/S0378-1097(97)00187-0)
 76. Argandoña M, Fernández-Carazo R, Llamas I et al (2005) The moderately halophilic bacterium *Halomonas maura* is a free-living diazotroph. *FEMS Microbiol Lett* 244:69–74. <https://doi.org/10.1016/j.femsle.2005.01.019>
 77. Yoshida N, Inaba S, Takagi H (2014) Utilization of atmospheric ammonia by an extremely oligotrophic bacterium, *Rhodococcus erythropolis* N9T-4. *J Biosci Bioeng* 117:28–32. <https://doi.org/10.1016/j.jbiosc.2013.06.005>
 78. Sañudo-Wilhelmy SA, Kustka AB, Gobler CJ, Hutchins DA, Yang M, Lwiza K, Burns J, Capone DG, Raven JA, Carpenter EJ (2001) Phosphorus limitation of nitrogen fixation by *Trichodesmium* in the central Atlantic Ocean. *Nature* 411:66–69
 79. Mackey KRM, Mioni CE, Ryan JP, Paytan A (2012) Phosphorus cycling in the red tide incubator region of Monterey Bay in response to upwelling. *Front Microbiol* 3:1–14. <https://doi.org/10.3389/fmicb.2012.00033>
 80. Hoffman BM, Lukoyanov D, Yang Z-Y, Dean DR, Seefeldt LC (2014) Mechanism of nitrogen fixation by nitrogenase: the next stage. *Chem Rev* 114:4041–4062. <https://doi.org/10.1021/cr400641x>
 81. Shi D, Xu Y, Hopkinson BM, Morel FMM (2010) Effect of ocean acidification on iron availability to marine phytoplankton. *Science* (80-) 327:676–679. <https://doi.org/10.1126/science.1183517>

82. Doney SC, Fabry VJ, Feely RA, Kleypas JA (2009) Ocean acidification: the other CO₂ problem. *Annu Rev Mar Sci* 1:169–192. <https://doi.org/10.1146/annurev.marine.010908.163834>
83. Kadam PC, Boone DR (1996) Influence of pH on ammonia accumulation and toxicity in halophilic, methylotrophic methanogens. *Appl Environ Microbiol* 62:4486–4492. <https://doi.org/10.1128/aem.62.12.4486-4492.1996>
84. Ge C, Chai Y, Wang H, Kan M (2017) Ocean acidification: one potential driver of phosphorus eutrophication. *Mar Pollut Bull* 115: 149–153. <https://doi.org/10.1016/j.marpolbul.2016.12.016>
85. Yu Plisova E, Balabanova LA, Ivanova EP, Kozhemyako VB, Mikhailov VV, Agafonova EV, Rasskazov VA (2005) A highly active alkaline phosphatase from the marine bacterium *Cobetia*. *Mar Biotechnol* 7:173–178. <https://doi.org/10.1007/s10126-004-3022-4>
86. Balabanova L, Golotin V, Kovalchuk S, Bulgakov A, Likhatskaya G, Son O, Rasskazov V (2014) A novel bifunctional hybrid with marine bacterium alkaline phosphatase and far eastern holothurian mannan-binding lectin activities. *PLoS One* 9:e112729. <https://doi.org/10.1371/journal.pone.0112729>
87. Weidberg N, Ospina-Alvarez A, Bonicelli J, Barahona M, Aiken CM, Broitman BR, Navarrete SA (2020) Spatial shifts in productivity of the coastal ocean over the past two decades induced by migration of the Pacific anticyclone and Bakun's effect in the Humboldt upwelling ecosystem. *Glob Planet Chang* 193:103259. <https://doi.org/10.1016/j.gloplacha.2020.103259>
88. Troncoso VA, Daneri G, Cuevas LA, Jacob B, Montero P (2003) Bacterial carbon flow in the Humboldt Current System off Chile. *Mar Ecol Prog Ser* 250:1–12. <https://doi.org/10.3354/meps250001>